Journal of Medicinal Chemistry

Article

Benzenesulfonamide Derivatives as Calcium/Calmodulin-Dependent Protein Kinase Inhibitors and Antiviral Agents Against Dengue and Zika Virus Infections

Wei-Chia Chen, Yogy Simanjuntak, Li-Wei Chu, Yueh-Hsin Ping, Yi-Ling Lee, Yi-Ling Lin, and Wen-Shan Li

J. Med. Chem., **Just Accepted Manuscript** • DOI: 10.1021/acs.jmedchem.9b01779 • Publication Date (Web): 23 Jan 2020

Benzenesulfonamide Derivatives as Calcium/Calmodulin-Dependent Protein Kinase Inhibitors and Antiviral Agents against Dengue and Zika Virus Infections

Wei-Chia Chen,[1,2,#] Yogy Simanjuntak,[3,#,*] Li-Wei Chu[4,5], Yueh-Hsin Ping[4,6], Yi-Ling Lee,[3] Yi-Ling Lin,[3,7,*] Wen-Shan Li[2,8,9,10*]

[1]Department of Chemistry, National Taiwan Normal University, Taipei 11677, Taiwan.

[2]Institute of Chemistry, Academia Sinica, Taipei 11529, Taiwan.

[3]Institute of Biomedical Sciences, Academia Sinica, Taipei 11529, Taiwan.

[4]Institute of Biophotonics, National Yang-Ming University, Taipei 11221, Taiwan.

[5]Reseach Center for Applied Sciences, Academia Sinica, Taipei 11529, Taiwan.

[6]Department and Institute of Pharmacology, National Yang-Ming University, Taipei 11221, Taiwan.

[7]Genomic Research Center, Academia Sinica, Taipei 11529, Taiwan.

[8]Doctoral Degree Program in Marine Biotechnology, National Sun Yat-Sen University, Kaohsiung 80424, Taiwan

[9]Ph.D Program in Biotechnology Research and Development, Taipei Medical University, Taipei 11031, Taiwan

[10]Department of Medicinal and Applied Chemistry, Kaohsiung Medical University, Kaohsiung 80708, Taiwan

ABSTRACT

Emerging and resurging mosquito-borne flaviviruses are an important public health challenge. The increased prevalence of dengue virus (DENV) infection has had a significant socio-economic impact on epidemic countries. The recent outbreak of Zika virus (ZIKV) has created an international public health emergency because ZIKV infection has been linked to congenital defects and Guillain-Barré syndrome. To develop potentially prophylactic antiviral drugs for combatting these acute infectious diseases, we have targeted the host calcium/calmodulin-dependent kinase II (CaMKII) for inhibition. By using CaMKII structure-guided inhibitor design, we generated four families of benzenesulfonamide (BSA) derivatives for SAR analysis. Among these substances, N-(4-cycloheptyl-4-oxobutyl)-4-methoxy-N-phenylbenzenesulfonamide (**9**) showed superior properties as a lead CaMKII inhibitor and antiviral agent. BSA **9** inhibited CaMKII activity with an IC_{50} value of 0.79 μM and displayed EC_{50} values of 1.52 μM and 1.91 μM against DENV and ZIKV infections of human neuronal BE(2)C cells, respectively. Notably, **9** significantly reduced the viremia level and increased animal survival time in mouse-challenge models.

INTRODUCTION

Dengue virus (DENV) and Zika virus (ZIKV) are mosquito-borne flaviviruses that pose a threat to global public health. DENV infection in humans is associated with a wide spectrum of clinical manifestations, which range from mild dengue fever to severe dengue hemorrhagic fever and life-threatening dengue shock syndrome[1]. A recent study estimated that DENV infection will reach 390 million cases per year[2]. Although the mortality rate has been controlled, recurrent dengue outbreaks have a significant socio-economic impact in epidemic countries[3]. Likewise, although the number of fatalities caused by ZIKV infection is low, ZIKV infection has been linked to onset of Guillain-Barré syndrome and to birth defects which include microcephaly[4, 5]. ZIKV infection has created an international public health emergency. It was reported that approximately 4300 infants were born with microcephaly during the recent outbreak in Brazil[4].

Both members of the *Flaviviridae* family, DENV and ZIKA possess envelopes and contain a positive-sense RNA genome encoding a polyprotein that is processed by cellular and viral proteases to form 3 structural (C, capsid; prM, precursor membrane; and E, envelope) and 7 nonstructural (NS1, NS2A, NS2B, NS3, NS4A, NS4B, and NS5) proteins[6, 7]. Viral infection begins with binding of the major structural envelope protein to the host cell receptor protein followed by entry of the virion into the cell by endocytosis. The internalized virions undergo acid-induced conformational changes and membrane fusion to release the viral genome. Translation of viral RNA produces proteins required for viral RNA replication through RNA-dependent RNA polymerization. The assembly of viral RNA and viral proteins generates the mature viral particle, which is then released through the cellular secretory pathway[6]. Flaviviruses exhibit a broad tissue tropism. Although

dendritic cells, monocytes/macrophages, and lymphocytes are considered the major sites of viral replication, some other cells can be permissive to flavivirus during natural infection including endothelial cells, neurons and microglia[6, 8, 9].

Antiviral drugs and vaccines are two major approaches to control viral diseases. Since most of the flavivirus infections result in acute diseases, the therapeutic window is narrow and short. Vaccine development for preventing flavivirus infection has been hampered in part by antibody-dependent enhancement. Preexisting antibodies that bind to E or prM of DENV or ZIKV have been shown to enhance viral infection of monocytes through Fc gamma receptors[10, 11]. For antiviral development, both viral and cellular proteins essential for viral replication serve as potential targets. Members of *Flaviviridae* may share similarities in their life cycles and host–pathogen interactions[12]. Our recent study indicated the role of calcium/calmodulin-dependent protein kinase II (CaMKII) in mediating the binding/entry of Japanese encephalitis virus (JEV), also a member of Flaviviridae[13]. JEV activated CaMKII via dopamine D2 receptor-phospholipase C signaling to increase the surface expression of JEV binding/entry molecule in neuronal cells. Therefore, CaMKII may serve as a suitable target for the development of prophylactic drug against flavivirus infection.

CaMKII is a serine/threonine-specific protein kinase that is regulated by the calcium and calmodulin complex[14]. Ubiquitously expressed in various tissues, CaMKII plays distinct roles in neurons, cardiomyocytes, endothelial and immune cells[14-16]. Owing to the elevated CaMKII activity associated with cardiovascular and brain disease[17, 18], pharmaceutical companies have initiated efforts to develop safe and effective therapeutics targeting CaMKII[17]. The goal of our studies in this area is to develop CaMKII inhibitors

that can be utilized to determine if this kinase is a viable antiviral drug target and if it can be used as a platform for antiviral drug design. The studies reported below demonstrated that N-(4-cycloheptyl-4-oxobutyl)-4-methoxy-N-phenylbenzenesulfonamide (**9**), is a novel CaMKII inhibitor that displays anti-DENV and anti-ZIKV activity in both cell and animal studies.

RESULTS AND DISCUSSION

Design and Synthesis of Benzenesulfonamides (BSAs) 1−16.

Several CaMKII inhibitors including KN-93 and KN-62 were developed previously to study the function of CaMKII[17]. In those investigations, it was observed that the presence of aromatic and sulfonamide groups in these substances is important for their inhibitory activities (**Chart 1**)[19]. Guided by these earlier findings, we designed several new BSAs derivatives that we proposed would be CaMKII inhibitors. These substances were prepared and their antiviral activities against DENV serotype 2 (DENV-2) and ZIKV infections were assessed.

Chart 1. Commercially available and widely used CaMKII inhibitors.

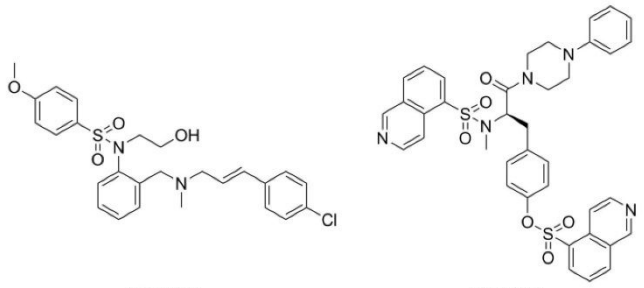

The final lead compounds, **1** and **2**, bearing sulfonamide and fluorobenzene moieties, were prepared by amide bond forming HBTU/DIPEA promoted condensation of keto-acid **17** with aniline (**Scheme 1**). Reduction of the formed amide **18** by using lithium aluminum hydride[20] produced amine **19**, which was utilized to form the target BSA **2** through reaction with 4-methoxybenzenesulfonyl chloride. BSA **1** was generated by oxidation of **2** with pyridinium dichromate in the presence of 4 Å molecular sieves[21].

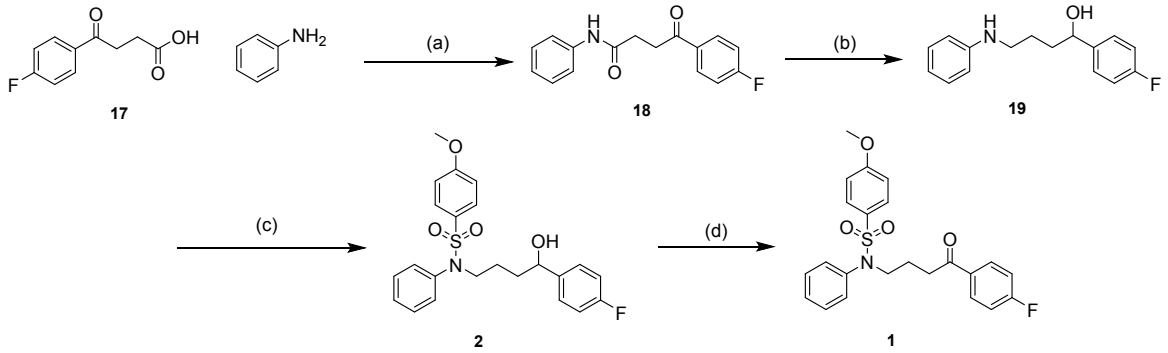

Scheme 1. Reagents, conditions and yields: **(a)** HBTU, DIPEA, THF, 8 h, rt, 92%; **(b)** $LiAlH_4$, THF, 4 h, 90 °C, 90%; **(c)** 4-methoxybenzenesulfonyl chloride, Et_3N, THF, 60 °C, 4 h, 75%; **(d)** PDC, DCM, 8 h, rt, 70%

BSAs **3** and **4**, analogs in which the *N*-phenyl moiety in **1** is replaced by H and CH_3, respectively, were synthesized by the routes shown in **Scheme 2**. In both sequences, amino-ketone **22** was prepared by reaction of chloride **20** with excess sodium azide and a catalytic amount of potassium iodide to form the intermediate azide **21**, followed by selective reduction using palladium on activated charcoal and hydrogen gas. Reaction of **22** with 4-methoxybenzenesulfonyl chloride furnished BSA **3**. Preparation of BSA **4** began with conversion of amine **22** to its *N*-methyl analog **23** through reductive methylation[22], and subsequent methoxybenzenesulfonamide formation.

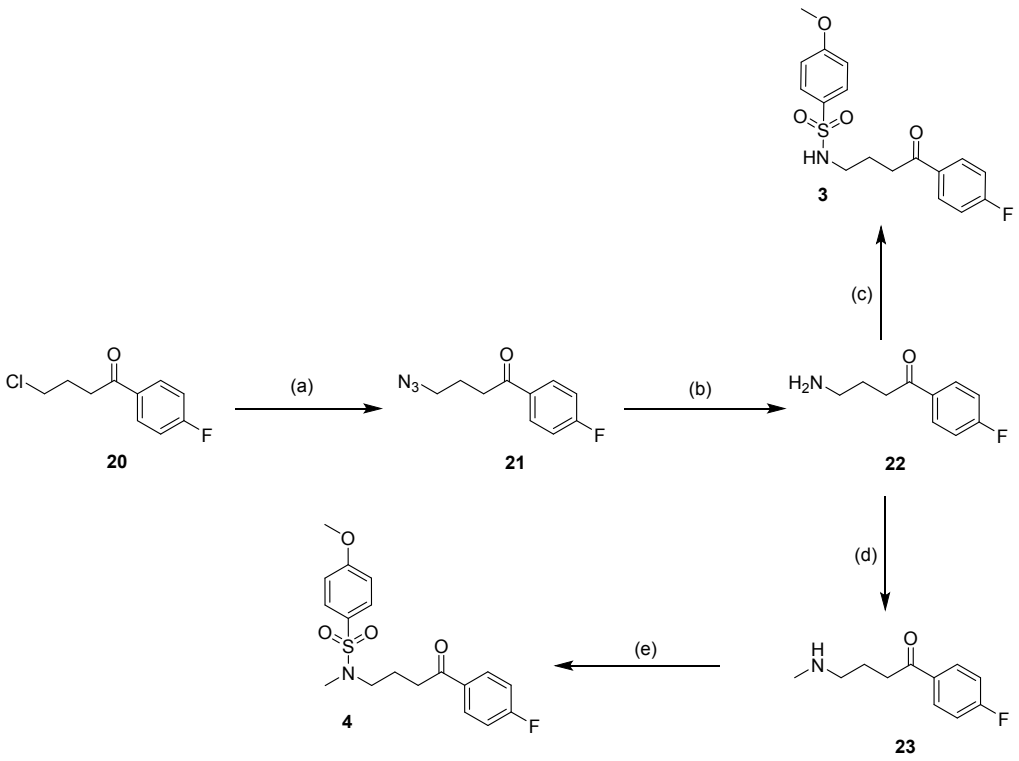

Scheme 2. Reagents, conditions and yields: **(a)** KI, NaN_3, DMF, 4 h, 90°C; **(b)** Pd/C, H_2, MeOH, 8 h, rt; **(c)** 4-Methoxybenzenesulfonyl Chloride, Et_3N, THF, 60°C, 4 h, 48%; **(d)** (1) HCHO, NaOMe, MeOH, 90°C, 4 h, (2) $NaBH_4$, MeOH, rt, 4 h, 63%; **(c)** 4-Methoxybenzenesulfonyl Chloride, Et_3N, THF, 60°C, 4 h, 78%

For structure–activity relationship studies, we designed and synthesized (**Scheme 3**) BSA derivatives **5-16**, which contain a variety of *para*-aryl and nitrogen substituents on the benzenesulfonamide moiety, and several different groups on the acyl carbon of the terminal ketone. The pathways for forming these BSAs began with reactions of the appropriate primary amines **24-27** with γ-butyrolactone[23] in the presence of sodium hydride at 90 °C to generate the corresponding amides **28-31**, which were reduced using $LiAlH_4$ to form the corresponding secondary amines **32-35**. Condensation reactions of these amines with selected aryl ring substituted benzenesulfonyl chlorides followed by oxidation with

pyridinium dichromate (PDC) afforded the respective aldehydes **43-49**. Finally, addition of excess amounts of the appropriate Grignard reagents[24, 25] to **43-49** gave secondary alcohols **50-56**, which were oxidized by using PDC to produce the respective BSAs **5-16**.

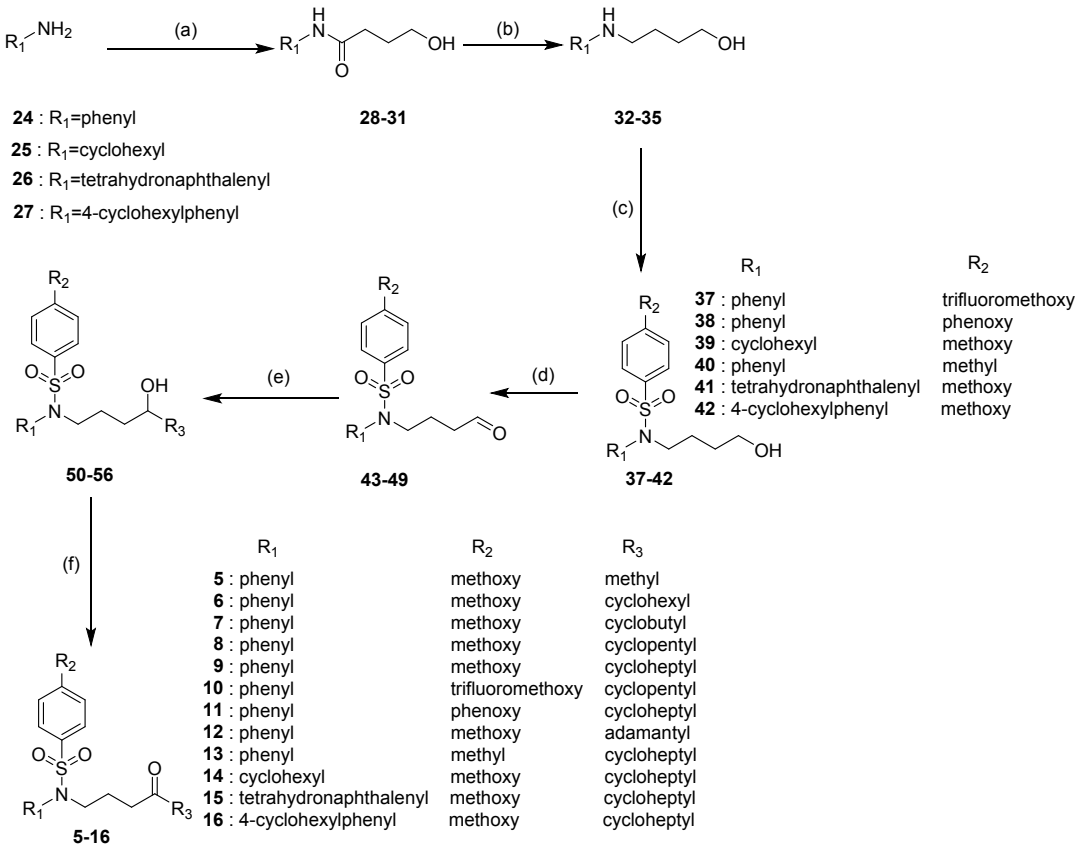

Scheme 3. Reagents, conditions and yields: **(a)** (1) NaH, THF, 30 min, 90 °C, (2) Butyrolactone, THF, 8 h, 90 °C, 90%; **(b)** $LiAlH_4$, THF, 8h, 90 °C; **(c)** Sulfonyl Chloride, Et_3N, THF, 60°C, 4 h, 76%; **(d)** PDC, DCM, 8 h, rt, 65%; **(e)** (1) R_2Br, Mg, THF, rt, 2 h, (2) Aldehyde, THF, 60 °C, 2 h, 60%; **(f)** PDC, DCM, 8 h, rt.

Structure–Activity Relationship Screening

BSAs **1-16** utilized in the SAR study contain four substructural units that correspond to the phenyl, terminal, linker and benzenesulfonamide parts depicted generally in **A** in **Figure 1**. The BSAs can be classified into four families (**B-E** in **Figure** 1) based on differences in these parts.

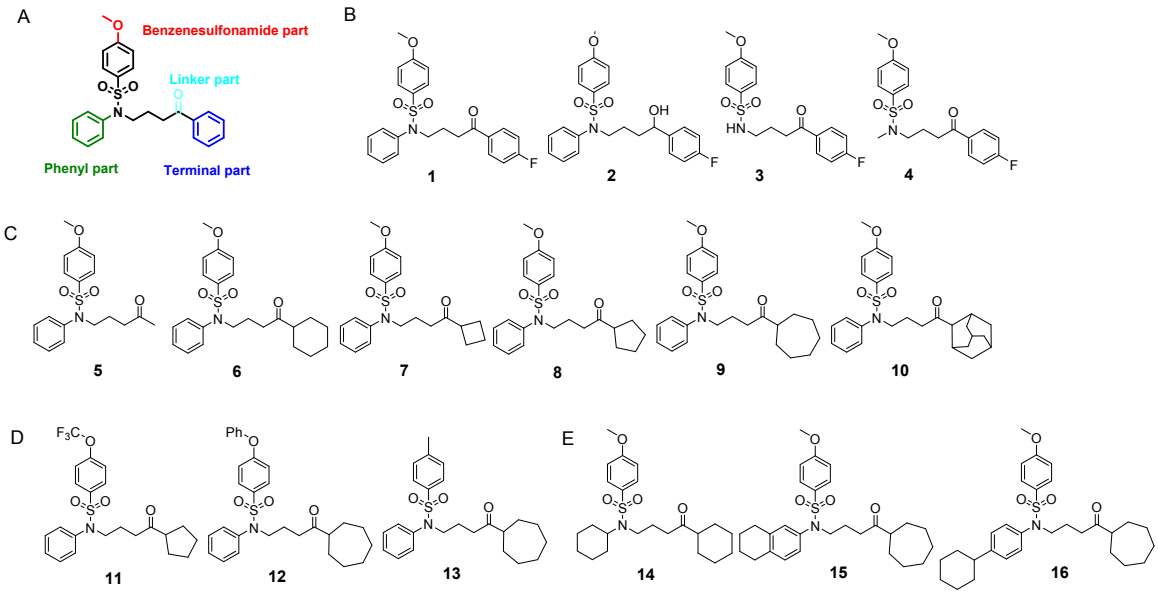

Figure 1. BSA **1** (A) and families of synthesized BSAs (B, C, D, E) used in the SAR study.

To assess the antiviral activities of the prepared BSAs, human neuroblastoma BE(2)C cells were infected with the DENV-2 reporter virus DENV-2-eGFP that expresses a green fluorescence protein. Specifically, BE(2)C cells in a 96-well plate were infected with DENV-2-eGFP and then incubated in the absence or presence of 1.56 and 3.13 μM of the BSAs for 24 h. DMSO was used as the solvent control. The antiviral activities of the compounds were determined by measuring the intensities of eGFP emission from the cells and are given in **Table 1** as percentages of cells infected relative to that of the solvent control. In addition, the effects of 6.25 μM of each BSA on hindrance of cell proliferation

(cytotoxicity) were determined by using the XTT assay and given in **Table 1** as a percentage of cell proliferation relative to that of the solvent control.

In studies with the BSAs in family **B** (**Figure 1**), we observed that treatment with BSA **1** resulted in only 39.3% of the BE(2)C cells being infected by DENV-2 and a 56.1% reduction of cell proliferation. In contrast, BSA **2** promoted only 48.5% cellular infection and had an improved effect (76.3%) on cell proliferation BSAs **3** and **4** did not cause a reduction in proliferation and had no antiviral potency against DENV-2 infection (**3** = 122.6%; **4** = 100.9%, **Table 1**). These data indicate that the benzene ring is required for anti-dengue activity of the BSA.

Table 1. Antiviral activities of the BSA, KN-62, and KN-93 against DENV-2-eGFP reporter virus and effect of BSA on cell proliferation.

BSA	Relative eGFP intensity of the infected-cells[a,b]		Cell proliferation of BSA treated-cells[a,c]
	BSA Concentration [1.56 μM]	[3.13 μM]	
1	55.9	39.3	56.1
2	59.4	48.5	76.3
3	110.1	122.6	105.7
4	100	100.9	105.9
5	92.8	100.8	105.9
6	68.9	63.3	106.6
7	42.8	33.0	93.9
8	34.6	25.1	90.0
9	31.8	9.6	90.0
10	57.3	51.1	96.7
11	102.6	118.2	92.4
12	74.7	73.4	95.5
13	93.9	76.9	99.5
14	85.7	65.7	97.5
15	87.2	21.5	103.6

16	36.1	13.8	100.4
KN-62	33.5	22.3	65.7
KN-93	30.5	14.5	84.3

[a] Values are means of 3 experiments (standard deviations were less than 10%).

[b] Normalized eGFP intensity of virus infected-cells treated with BSA to the solvent-treated cells (%).

[c] Normalized proliferation of non-infected cells treated with 6.25 μM of the BSA to solvent control (%).

Building on these findings were observations made in studies of BSAs in family C where the terminal part is modified (**Figure 1**). The methylketone **5** displayed no effect on DENV infection (100.8% infection, **Table 1**), while its cyclohexyl analog **6** has an observable antiviral potency that is less than that of **1** (**1** = 39.3% vs **6** = 63.3, **Table 1**). Moreover, the terminal cyclobutyl (**7**) and cyclopentyl (**8**) substituted BSAs had antiviral activities that are similar to those of **1** (and **7** = 33% and **8** = 25.1%, **Table 1**). Notably, **7** and **8** had greatly improved cytotoxicity as compared with that of **1** (**Table 1**). In contrast, the cycloheptyl substituted BSA **9** displayed a remarkable effect in reducing DENV-2 infection (9.6%) and a minor effect on cell proliferation (**Table 1**), while the adamantyl substituted analog **10** displayed 51.1% activity against DENV-2 infection and only minor effect on cell proliferation (**Table 1**).

In investigations with BSAs in family **D** where the methoxy group on the benzenesulfoamide group in **1** is modified, we found that the trifluoromethoxy (**11**), phenoxy (**12**) and methyl (**13**) derivatives have either no (**11** = 118.2%), or little (**12** = 73.4%, and **13** = 76.9%) effect on DENV-2 infection and only minor effects on cell proliferation (**Table 1**). Likewise, other changes made in the substituents in the BSAs

brought about only minor changes in the effect against DENV-2 infection (**14** = 65.7%, **15** = 21.5% and **16** = 13.8%). Notably, the known allosteric inhibitors KN-62 and KN-93 showed a relatively comparable anti-DENV effect with **8** and **9** (**Table 1**). However, KN-62 and KN-93 reduced cell proliferation to ~16-35%, greater than that of **8** or **9** (**Table 1**).

Taken together, the highest levels of anti-DENV activity occur when the BSAs contain a *N*-phenyl and a *para*-methoxy group on the benzenesulfonamide group. Significantly, the cycloheptyl-ketone **9**, which contains these features, has the highest antiviral activity and lowest cytotoxicity of the BSA derivatives examined.

BSA 9 Inhibits DENV-2 and ZIKV Infection In Vitro

Next, we evaluated the potency of **9** against wild-type DENV-2 infection of human neuronal BE(2)C cells. We first carried out a comprehensive evaluation of **9** for cell toxicity by employing 3 different assays including the LDH cytotoxicity assay, XTT cell proliferation assay and trypan blue viable cell counting assay. Tested at a concentration up to 12.5 μM against BE(2)C cells, **9** had no significant effect on cytotoxicity, cell proliferation, or cell viability (**Figure 2A**). Importantly, in the case of DENV-2 infection, treatment of cells with **9** significantly reduced the expression of DENV-2 NS3 protein, as well as viral progeny production, in a dose-dependent manner (**Figure 2B-D**), with an EC_{50} of 1.52 μM. In the case of ZIKV infection, cell treatment with **9** significantly inhibited ZIKV-E protein expression and viral progeny production (**Figure 2E-G**), with an EC_{50} of 1.91 μM. Thus, at noncytotoxic concentrations, **9** showed antiviral effects against DENV-2 and ZIKV infections in BE(2)C cells. To evaluate whether **9** also displays antiviral effect in other cell type, we tested the antiviral activity of **9** against DENV-2 and ZIKV in human microglial HMC3 cells. Treatment with noncytotoxic doses of **9** significantly reduced the

expression of viral NS3 protein and the level of progeny production in HMC3 cells (**Figure S1**). Furthermore, **9** might display antiviral effect against other viruses that also employ endocytosis-mediated viral entry including influenza A H1N1 and sindbis virus (SINV)[26]. Treatments with **9** greatly reduced the expression of nucleoprotein (NP) in H1N1-infected cells and the GFP reporter of SINV-infected cells (**Figure S2**).

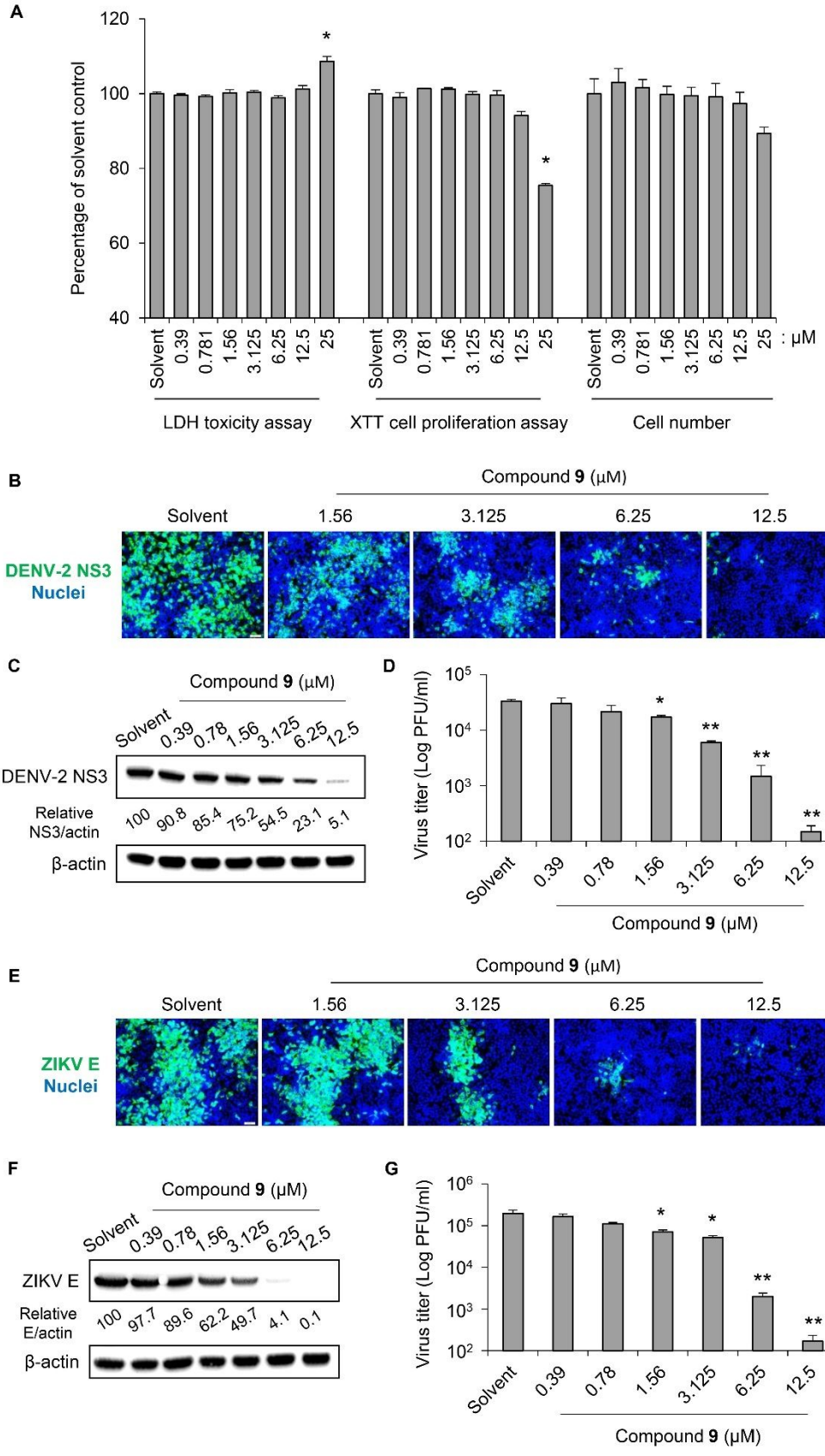
A
Percentage of solvent control
120
100
80
60
40
*
*
Solvent
0.39
0.781
1.56
3.125
6.25
12.5
25
: μM
LDH toxicity assay
XTT cell proliferation assay
Cell number
B
Compound 9 (μM)
Solvent
1.56
3.125
6.25
12.5
DENV-2 NS3
Nuclei
C
Compound 9 (μM)
Solvent
0.39
0.78
1.56
3.125
6.25
12.5
DENV-2 NS3
Relative NS3/actin
100
90.8
85.4
75.2
54.5
23.1
5.1
β-actin
D
Virus titer (Log PFU/ml)
10^5
10^4
10^3
10^2
*
**
**
**
Solvent
0.39
0.78
1.56
3.125
6.25
12.5
Compound 9 (μM)
E
Compound 9 (μM)
Solvent
1.56
3.125
6.25
12.5
ZIKV E
Nuclei
F
Compound 9 (μM)
Solvent
0.39
0.78
1.56
3.125
6.25
12.5
ZIKV E
Relative E/actin
100
97.7
89.6
62.2
49.7
4.1
0.1
β-actin
G
Virus titer (Log PFU/ml)
10^6
10^5
10^4
10^3
10^2
*
*
**
**
Solvent
0.39
0.78
1.56
3.125
6.25
12.5
Compound 9 (μM)

Figure 2. Determination of the cytotoxicity and antiviral activity of **9** against DENV-2 and ZIKV infection (multiplicity of infection [MOI], 0.1). (**A**) The percentage ratio of the fraction of viable BE(2)C cells treated with **9** relative to that of the solvent control determined by using the LDH cytotoxicity assay (left panel), XTT cell proliferation assay (center panel), and trypan blue viable cell counting assay (right panel). (**B**) Immunofluorescence microscope imaging (200x magnification) of DENV-2 NS3 (green) in DENV-2-infected BE(2)C cells treated with **9** for 48 h at increasing concentration. Nuclei are stained blue. (**C**) Western blot of DENV-2 NS3 in DENV-2-infected BE(2)C cells treated with **9** at increasing concentration. Actin served as the loading control. The reported values of the ratios of DENV-2 NS3:actin band densities are listed as percentages of the ratio determined for the solvent control. (**D**). Virus titer determined for DENV-2-infected BE(2)C cells treated with **9** at increasing concentration. (**E**) Immunofluorescence microscopic imaging (200x magnification) of ZIKV E (green) in ZIKV-infected BE(2)C cells treated for 48 h with **9** at increasing concentration. Nuclei are stained blue. (**F**) Western blot of ZIKV E in ZIKV-infected BE(2)C cells treated with **9** at increasing concentration. Actin served as the loading control. The reported values of the ratios of ZIKV E: actin band densities are listed as percentages of the ratio determined for the solvent control. (**G**) Virus titer determined for ZIKV-infected BE(2)C cells treated with **9** at increasing concentration. Values are reported as the mean ± standard deviation of 3 independent experiments. *$P < 0.05$ and **$P < 0.01$, compared with solvent control.

Compound 9 Blocks Cellular Entry of DENV-2 and ZIKV

To determine the mechanism for the antiviral action of **9**, we investigated whether **9** inhibits the early (0-3 hpi) or late (3-24 hpi) stages of viral infection. As revealed by the results shown in **Figure 3A**, within early but not late stage of infection, **9** promoted a significant reduction in DENV-2 NS3 expression in a dose dependent manner. Therefore, to further examine the mechanism of action, we focused on the early steps of viral infection by performing virus-binding and virus-entry assays (see "Experimental Section" for details). Treatment of BE(2)C cells with **9** had no effect on DENV-2 and ZIKV binding (**Figure 3B**). However, the levels of DENV-2 and ZIKV entry were significantly reduced by **9** in a concentration-dependent manner up to 70% and 80% reduction, respectively (**Figure 3C**). **9** also greatly reduced the signal from fluorescently labeled DENV-2 and ZIKV within the cells as compared with that from control cells treated with solvent only (**Figure 3D** and **3E**). Thus, the antiviral effect of **9** against DENV-2 and ZIKV infection derives from inhibition of viral entry into the host cell.

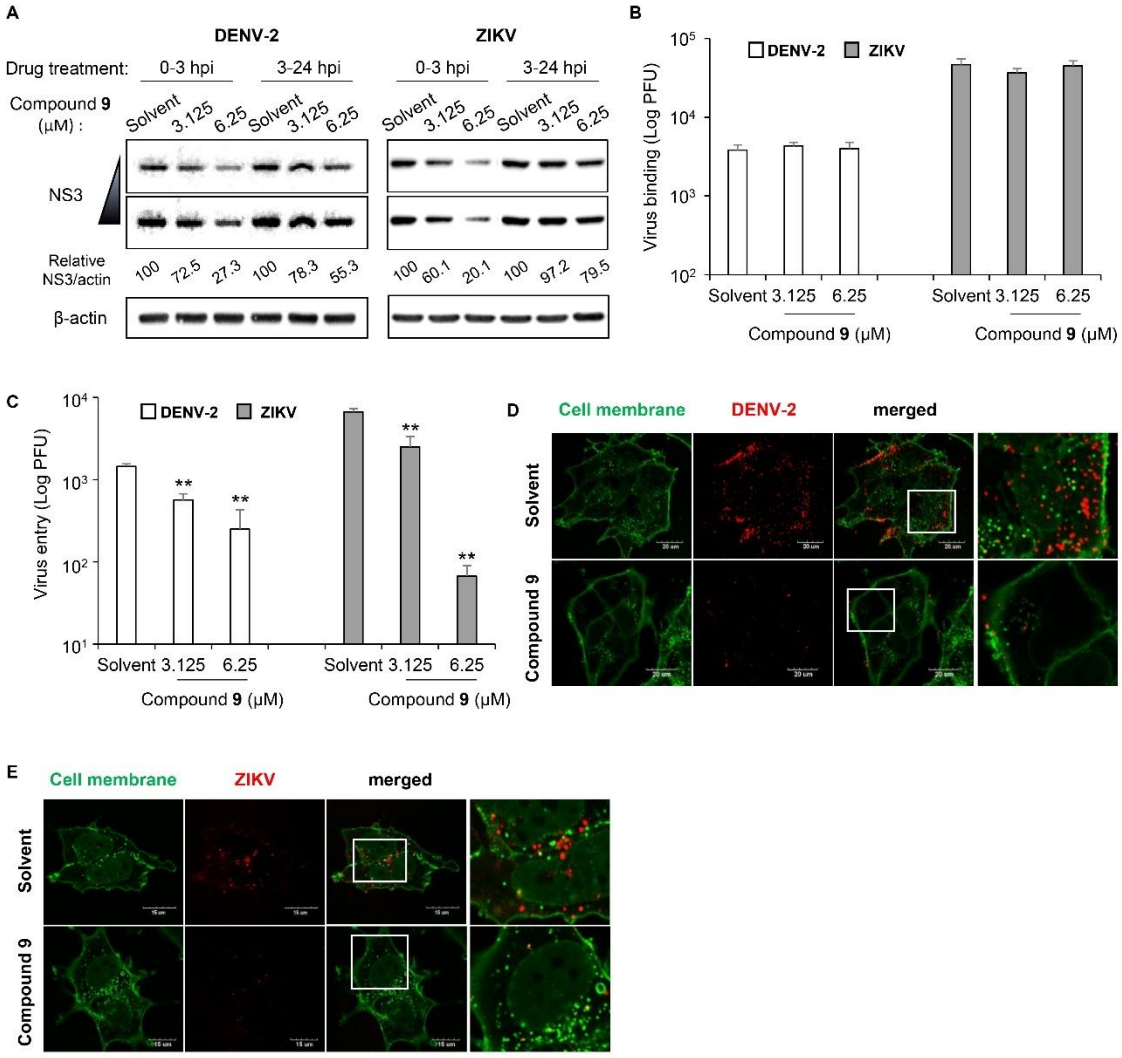

Figure 3. The effect of **9** on the DENV-2 and ZIKV cell binding and entry. (**A**) Western blot of DENV-2 NS3, ZIKV E, and the loading control actin. BE(2)C cells were infected with DENV-2 or ZIKV (MOI, 1) in the absence or presence of 3.125 or 6.25 μM **9** during (0-3 hpi) or after (3-24 hpi) virus adsorption. The reported ratios of the viral protein: actin band densities are reported as percentages of the ratio determined for the solvent control. (B) The level of DENV-2 or ZIKV binding to exposed BE(2)C cells determined in the absence or presence of 3.125 or 6.25 μM **9**. Data are mean ± standard deviation of 3 independent experiments. (C) The level of DENV-2 or ZIKV entry to exposed BE(2)C

cells determined in the absence or presence of 3.125 or 6.25 μM **9,** using the plaque-forming assay. Values are mean ± standard deviation of 3 independent experiments. **P <0.01, compared with solvent control. (**D**) and (**E**) Representative confocal microscope images of fluorescently-labeled DENV-2-infected (D, scale: 20 μm) and ZIKV-infected (E, scale: 15 μm) BE(2)C cells treated with 3.125 μM **9** or solvent (control). The labeled viruses are red and the stained cell membranes are green.

BSA 9 Increases the Survival Time of DENV-2- and ZIKV-Infected Mice

For the purpose of testing the impact of **9** on the survival of mice infected with DENV-2 or ZIKV, we used *Stat1*$^{-/-}$ mice which exhibit paralysis, hemorrhage, vascular leakage and death after being challenged with a mouse-adapted DENV-2 NGC-N strain[27]. STAT1 is a transcriptional factor activated by various cytokines, and disruption of the mouse *Stat1* gene results in compromised innate immunity against viral diseases[28]. Oral treatment with **9** at doses of 4 or 8 mg/kg body weight immediately following DENV-2 infection, and then daily for a 6 d period, increased the overall mouse survival number from 0% to 60% (**Figure 4A**). Notably, immediate treatment with a lower dose of **9** (2 mg/kg body weight/day) significantly delayed animal mortality (T_{50}, 15 days vs 9 days for the vehicle control), with a minor effect on overall animal survival (**Figure 4A**).

Oral treatment with **9** at a dose of 8 mg/kg body weight immediately following ZIKV infection, and then daily for a 6 d period, significantly delayed ZIKV-induced lethality as reflected in the increase in the median survival time T_{50} from 13 d to 18 d (**Figure 4B**). However when used at the lower dose of 4 mg/kg body weight, **9** did not improve the survival time (**Figure 4B**).

Consistent with the improvements observed in mouse survival rate as a result of immediate treatment with **9**, we found that the viral load of DENV-2 or ZIKV-infected mice was significantly reduced as a result of treatment with **9** (**Figure 4C**). Taken together, these findings provide strong evidence that **9** displays antiviral activity against DENV-2 and ZIKV infections.

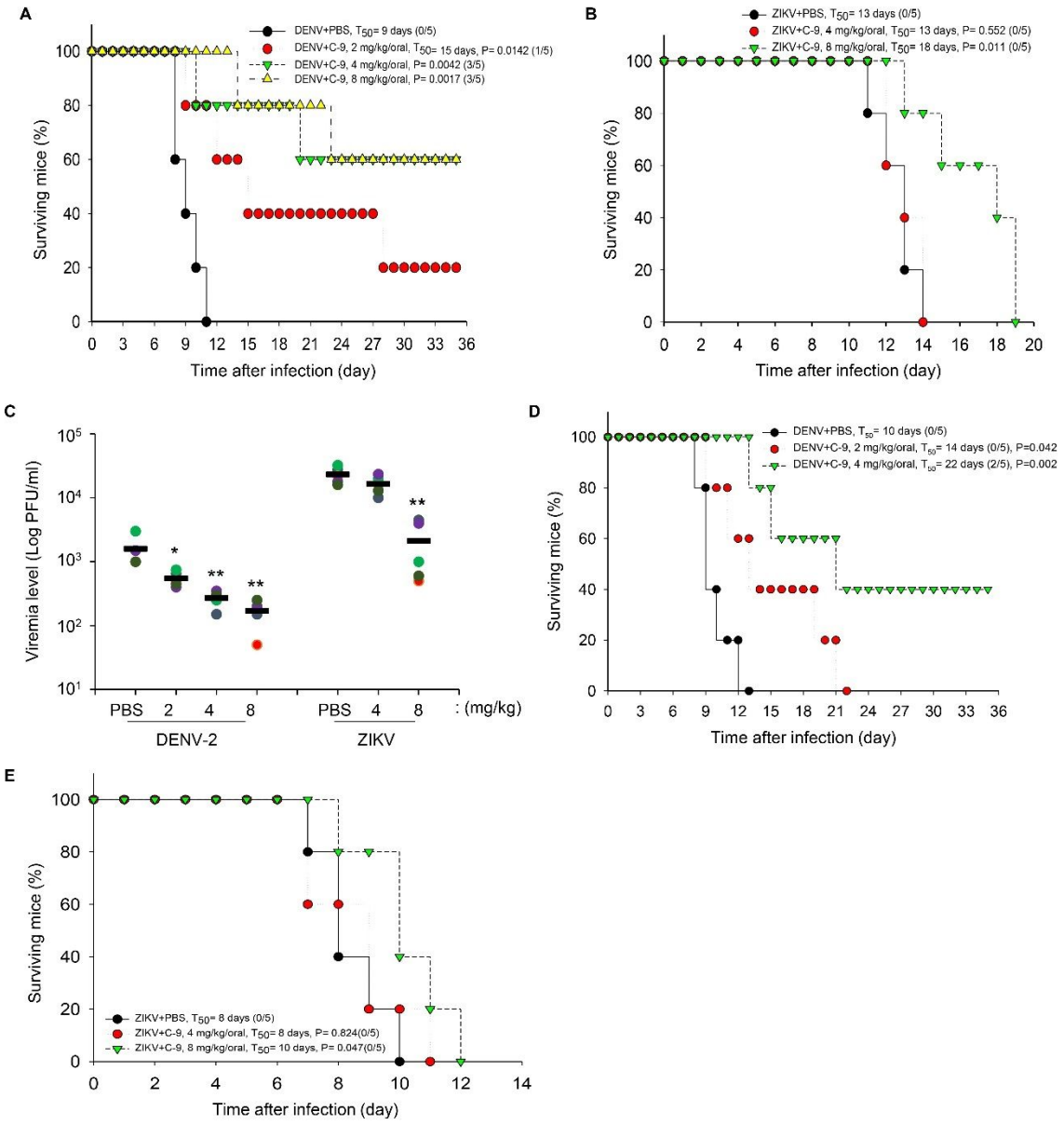

Figure 4. The impact of **9** on viral load and survival time for DENV-2 and ZIKV-infected Stat1$^{-/-}$ mice. (**A**) Percent of mice surviving during the course of 36 d after infection with DENV-2 and immediate initiation of a 6 d oral treatment with phosphate-buffered saline (PBS; n = 5) (control) or **9** at doses of 2, 4 or 8 mg/kg body weight (n = 5). (**B**) Percent of mice surviving during the course of 22 d after infection with ZIKV and immediate initiation of a 6 d oral treatment with PBS (n = 5) or **9** at doses of 4 or 8 mg/kg body weight (n = 5). (**C**) Viremia levels determined for serum samples assayed on day 3 following the infection of Stat1$^{-/-}$ mice with DENV-2 or ZIKV and immediate treatment with **9**. The control and the doses of **9** used in these experiments are the same as those stated in (A) and (B). The viremia levels are reported as the mean (black bar) and individual data (circle, n = 5). The $*P < 0.05$ and $**P < 0.01$, compared with solvent control. **(D)** Percent of mice surviving during the course of 36 d after infection with DENV-2 and an 8 h delay in the initiation of the 6 d daily treatment with **9**. The control and doses of **9** used in these experiments are the same are the same as those listed in (A) with the exception of the 8 mg/kg dose. (**E**) Percent of mice surviving during the course of 12 d after infection with ZIKV and an 8 h delay in the initiation of the 6 d daily treatment with **9**. The control and doses of **9** used in these experiments are the same as those listed in (B). The median survival times (T_{50}) reported in the figures were determined using the log-rank test.

Using a therapeutic mode, which involves starting administration of the agent 8 h after infection and ending at day 6 after infection (8-h-delay), we found that treatment with 2 mg of **9**/kg body weight/day was sufficient to significantly improve the median survival time of DENV-2-infected mice from 10 d to 14 d (**Figure 4D)**. Moreover, treatment with

a higher dose of **9** (4 mg/kg body weight/day) increased the overall survival to 40% and the median survival time from 10 to 22 d (**Figure 4D)**. However, using a 8-h-delay treatment of ZIKV-infected mice with **9** resulted in only a minor improvement in the median survival time from 8 to 10 d, and had no impact on overall survival (**Figure 4E**). The difference in virulence and/or viral pathogenesis between DENV-2 and ZIKV in *Stat1*-deficient mice may contribute to the differences observed in the effectiveness of **9** towards delaying or preventing death. Intriguingly, the inhibitory effect of **9** on the early stage of DENV-2 and ZIKV infection may explain the greater efficacy of compound **9** observed when administered immediately following infection rather than 8 h after infection.

BSA 9 inhibits CaMKIIα activity

Previous studies have demonstrated that JEV, enterovirus 71 (EV71), and rabies virus infection activates CaMKII[13, 29, 30]. Activation of CaMKII enhances actin assembly and the formation of surface focal adhesion including αvβ3 integrin[31]. In addition, activation of CaMKII further phosphorylates vimentin[30]. Notably, actin rearrangement, integrin β3, and vimentin play important roles in flavivirus entry and/or binding[13, 32-34]. CaMKII is activated by the binding of the calcium/calmodulin complex to the C-terminal region of the regulatory domain. This, in turn, displaces the regulatory domain to facilitate access of substrates to the active site of the kinase domain. In addition, the binding of calcium/calmodulin to the regulatory domain mediates the autophosphorylation of Thr286, which impairs the rebinding of regulatory domain to the active site of the kinase domain. Thr286 autophosphorylation is greatly enhanced by binding of ATP to the ATP-binding site within the active site of the kinase domain[14, 17, 35].

Molecular docking studies were carried out with **9** and CaMKIIα to identify the most probable binding site. As illustrated in **Figure 5A**, consistent with our expectation, we found that **9** is predicted to bind to the active site located at the interface between the N-lobe and C-lobe of the CaMKIIα kinase domain (**Figure 5A**). Here, the sulfonamide group of **9** is positioned to form hydrogen bonds with the backbone amide NH of Ala23 (2.21 Å) and of Phe24 (2.31 Å) (**Figure 5B**; green line). Hydrophobic interactions with **9** involve the nonpolar regions of Lys21, Gly22, Glu139, Gly175, and Gly158 (**Figure 5B**; red line). Notably, Lys21, Gly22, and Phe24 are located within the ATP-binding site[36] and Glu139 is required for binding the protein substrate[37].

Intriguingly, cycloheptyl feature in the terminal part of BSA may improve the antiviral activity. To support this notion, we further performed docking analysis of **8**, **7**, and **6** with CaMKIIα. BSA **8**, **7**, and **6** showed less and less interactions with CaMKIIα than **9** (**Figure S3A-D**). The binding free energy (MM/PBSA) of **9**-, **8**-, **7**-, and **6**-CaMKIIα was -65.545, -61.257, -62.294, and -52.295 KJ/mol, respectively (**Figure S3A-D**). We further evaluated the probable interactions of **9** with other kinases that play a role in early steps of DENV-2 and/or ZIKV infection including tyrosine kinase Axl, tyro3, and p38 mitogen-activated protein kinase (p38MAPK)[38, 39]. There were hydrophobic interactions between **9** and the kinase domain of Axl, tyro3 or p38MAPK. However, the interactions were poor and required a relatively higher free energy binding as compared with that of CaMKIIα (**Figure S3E-G**).

BSA **9** was tested in parallel with the known allosteric inhibitor KN-62, to determine its ability to inhibit the activity of human CaMKIIα. The results obtained (**Figure 5C**) confirm the requirement for Ca^{2+} for activation and show that **9** has an IC_{50} =

0.79 μM and KN-62 IC_{50} = 1.03 μM. Moreover, **8** and **16** that displayed slightly lower potency of anti-DENV effect than **9** also inhibited CaMKIIα activity with IC_{50} = 0.84 μM and 0.81 μM, respectively (**Figure S4**). Notably, **2** and **3** that showed intermediate or no anti-DENV effect also could reduce CaMKIIα activity but it required a relatively higher concentration as compared with **9**, **8**, or **16** (**Figure S4**). Thus, the antiviral property of BSAs may correlate with their potency to inhibit CaMKIIα activity.

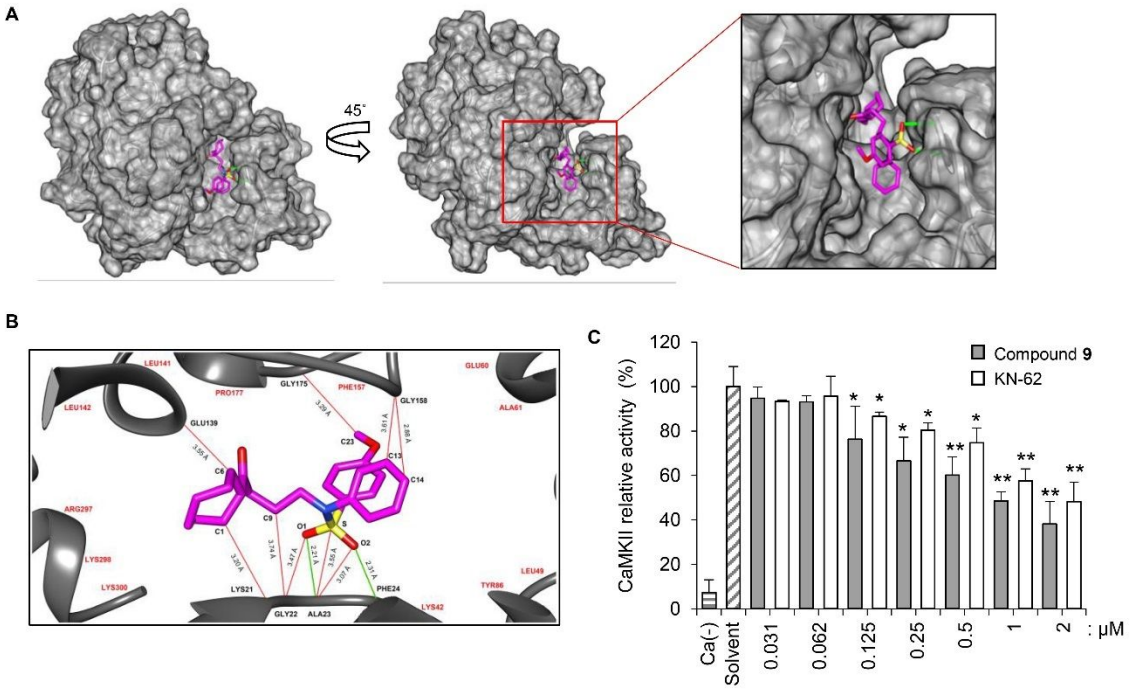

Figure 5. CaMKII-**9** Molecular docking and inhibition. (**A**) Predicted docking conformation of **9** in complex with human CaMKIIα (2VZ6.pdb). (**B**) Hydrogen-bonding (green line) and hydrophobic interactions (red line) between **9** and the CaMKIIα binding site residues (black font). (**C**) Inhibition of CaMKIIα activity with **9** and KN-62. Data are mean ± standard deviation (n = 3). *P < 0.05 and **P < 0.01, compared with the solvent control.

The antiviral effect of BSA 9 is associated with CaMKIIα expression

Lastly, we evaluated whether the expression of CaMKIIα is essential for the antiviral property of **9**. The mode of antiviral action of **9** was by inhibiting viral entry, so we monitored the activation of CaMKIIα at the early time of DENV-2 and ZIKV infection. DENV-2 and ZIKV infection for 4 hours significantly increased the level of phosphorylated-CaMKIIα (**Figure 6A** and **6B**). Treatment with 3.125 μM **9** greatly repressed the viral induced-CaMKIIα activation (**Figure 6A** and **6B**). Next, we established CaMKIIα-deficient BE(2)C cells by transduction with a lentivirus expressing shRNA-targeting CaMKIIα (shCaMKIIα) (**Figure 6C**). The level of DENV-2 and ZIKV NS3 protein and progeny production in shCaMKIIα-BE(2)C cells was greatly lower than that of BE(2)C and shLacZ-BE(2)C control cells (**Figure 6D** and **6E**). Importantly, treatments with **9** significant repressed the infection of DENV-2 and ZIKV in shLacZ-BE(2)C control cells, whereas **9** displayed minor antiviral effects in shCaMKIIα-BE(2)C cells (**Figure 6F-I**). This data suggested that antiviral property of **9** against DENV-2 and ZIKV was associated with CaMKIIα expression.

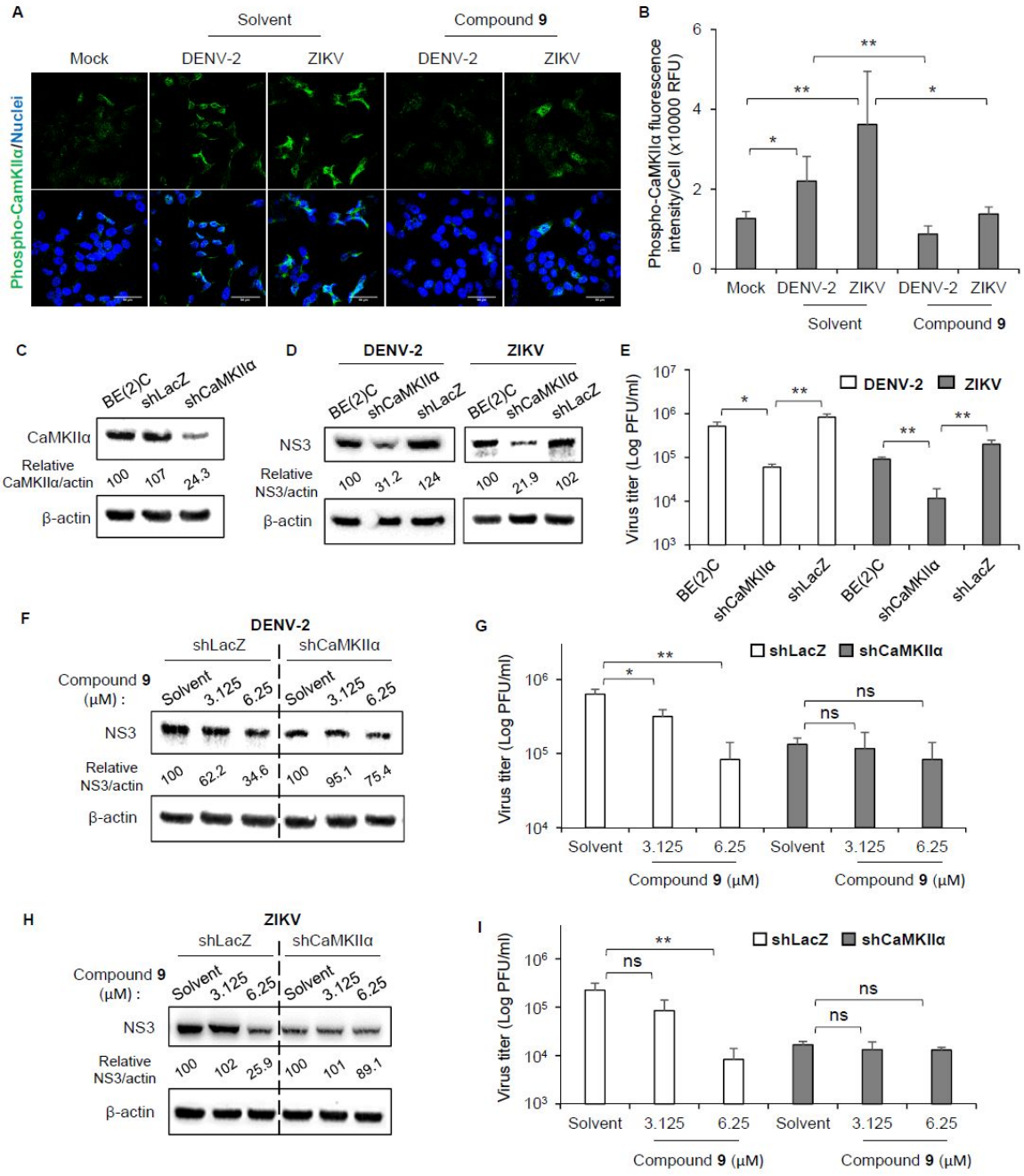

Figure 6. The antiviral activity of BSA9 is associated with CaMKIIα expression. (**A-B**) BE(2)C cells were infected with DENV-2 or ZIKV (MOI, 10) in the absence or presence of 3.125 μM **9** for 4 h. Representative confocal microscope images of phosphorylated-CaMKIIα (green) and nuclei (blue) of the cells (A, scale: 50 μm). Relative fluorescence intensity of phosphorylated-CaMKIIα per cell based on high content image analysis (B).

(**C**) Western blot analysis of knockdown efficiency of CaMKIIα. (**D-E**) Cells were infected with DENV-2 or ZIKV (MOI, 5) for 24 h. Western blot of DENV-2 and ZIKV NS3. Actin served as the loading control (D). Virus titer for DENV-2- or ZIKV-infected cells (E). (**F-G**) Cells were infected with DENV-2 (MOI, 5) in the absence or presence of 3.125 or 6.25 μM 9 for 24 h. Western blot of DENV-2 NS3 and the loading control actin (F). Virus titer for the respective DENV-2-infected cells (G). (**H-I**) Cells were infected with ZIKV (MOI, 5) in the absence or presence of 3.125 or 6.25 μM 9 for 24 h. Western blot of ZIKV NS3 and the loading control actin (H). Virus titer for the respective ZIKV-infected cells (I). The reported ratios of the CaMKII or viral NS3 protein:actin band densities are reported as percentages of the ratio determined for the BE(2)C (C), BE(2)C-infected control (D), or respective solvent control (F and H). Data are mean ± standard deviation of 3 independent experiments. *$P < 0.05$ and **$P < 0.01$, compared with control. ns: not significant.

CONCLUSION

We developed the novel benzenesulfonamide derivative **9** to inhibit CaMKII activity. BSA **9** was shown to display anti-DENV-2 and -ZIKV effects during the early step of viral infection with an EC_{50} of 1.52 μM and 1.91 μM, respectively. Importantly, **9** reduces the viremia level and improves the survival of both DENV-2 and ZIKV-infected mice. In vitro inhibition studies demonstrated that **9** inhibits the catalytic activity of human CaMKIIα with an EC_{50} of 0.79 μM. Molecular docking results indicate that **9** might exert its inhibitory effect by binding to the CaMKIIα active site.

EXPERIMENTAL SECTION

Chemistry: All reagents and solvents were obtained from commercial sources and used as purchased unless otherwise stated. THF was freshly distilled from Na/benzophenone ketyl under a nitrogen atmosphere. ^{1}H NMR and ^{13}C NMR spectra were recorded on Bruker AVIII-400, AV-400 or AV-500. Proton chemical shifts are reported in parts per million (ppm) relative to the singlet at 7.24 ppm for residual $CHCl_3$ in the deuteriochloroform. Carbon chemical shifts were reported in parts per million relative to the internal ^{13}C signals in the $CDCl_3$ (77.0 ppm) and acetone-d_6 (29.1 ppm) resonances. High resolution mass spectra were obtained with Waters LCT Premier XE (Waters Corp., Manchester, UK) and Bruker, New ultrafleXtremeTM, Bremen, D.E. Analytical thin layer chromatography (TLC) was performed on silica gel 60 F_{254} (Merck). Column chromatography was performed with silica gel 60 (230–400 mesh) (Merck). The purity of compounds was established as >95% by using normal phase HPLC, Waters 1525 Binary System with a Waters 2489 dual λ absorbance detector at 254 nm for all compounds; eluent, ethyl acetate and hexane; column Purospher STAR Si (5 μm), Merk and Venusil XBP Silica, Agela Technologies.

***N*-(4-(4-Fluorophenyl)-4-oxobutyl)-4-methoxy-N-phenylbenzenesulfonamide (1)**

A solution of pyridinium dichromate (0.91 g, 2.43 mmol) and **2** (0.8 g, 1.87 mmol) in DCM (30 mL) containing 4 Å molecular sieves (1.0 g) was stirred at room temperature for 8 h. The mixture was diluted with ethyl acetate and water, and separated. The combined organic layers were dried over magnesium sulfate and concentrated in vacuum. The residue was subjected to flash column chromatography, followed by normal-phase HPLC to afford the pure **1** as a white solid (70%): mp 93−94 °C. ^{1}H NMR (400 MHz, $CDCl_3$) δ 1.82-1.89 (m,

2H), 3.09-3.12 (t, *J* = 7.2 Hz, 2H), 3.66-3.69 (t, *J* = 6.0 Hz, 2H, 3.87 (s, 3H), 6.94 (d, *J* = 8.4 Hz, 2H), 7.09 (d, *J* = 7.2 Hz, 2H), 7.13 (t, *J* = 8.4 Hz, 2H), 7.32 (d, *J* = 6.4 Hz, 2H), 7.51 (d, *J* = 8.0Hz, 2H), 7.97 (t, *J* = 7.2 Hz, 2H); ^{13}C NMR (100 MHz, $CDCl_3$) δ 22.25, 35.00, 49.63, 55.58, 113.96, 115.54, 115.72, 127.96, 128.68, 129.10, 129.75, 130.61, 130.68, 133.27, 138.98, 162.91, 164.69, 166.71, 197.75 HRMS (ESI) calcd for $C_{23}H_{22}NO_4FS$ $(M + Na)^+$, 450.1151; found, 450.1146.

***N*-(4-(4-Fluorophenyl)-4-hydroxybutyl)-4-methoxy-N-phenylbenzenesulfonamide (2)**

A solution of aniline (2 mL, 21.93 mmol), acid **17** (4.30 g, 21.93 mmol), HBTU (9.15 g, 24.12 mmol), and DIPEA (7.64 mL, 43.86 mmol) in THF (60 mL) was stirred at room temperature for 8 h. The mixture was concentrated under reduced pressure and the residue was subjected to column chromatography to obtain **18** as a white solid (5.47 g, 92%).

A solution of **18** (2.00 g, 7.36 mmol) in THF (10 mL) was added dropwise over 30 min period to a suspension of lithium aluminum hydride (696 mg, 18.40 mmol) in dry THF (20 mL) at 0 ^{o}C under argon.. The mixture was then stirred at 90 ^{o}C for 8 h, and diluted with ethyl acetate and water. The organic layer was separated, dried over magnesium sulfate and concentrated in vacuum giving **19** as a gray oil (1.72 g, 90%), which was used in next step without further purification.

A solution of 4-methoxybenzenesulfonyl chloride (1.59 g, 7.71 mmol), triethylamine (2.15 mL, 15.42 mmol) and **19** (2 g, 7.71 mmol) in THF (60 mL) was stirred at 60 ^{o}C for 8 h. The mixture was diluted with ethyl acetate and water, and separated. The combined organic layers were dried over magnesium sulfate and concentrated in vacuum. The residue was subjected to flash column chromatography, followed by normal-phase

HPLC to afford pure **2** as a colorless oil (2.48 g, 75%). ^{1}H NMR (400 MHz, $CDCl_3$) δ 1.42-1.54 (m, 2H), 1.78-1.84 (m, 2H), 3.55-3.60 (m, 2H), 3.88 (s, 3H), 4.68 (t, *J* = 6.4 Hz, 2H), 6.92 (d, *J* = 8 Hz, 2H), 7.01 (d, *J* = 13.6 Hz, 2H), 7.03 (d, *J* = 8.4 Hz 2H), 7.26-7.29 (m, 3H), 7.51 (d, *J* = 8.4 Hz, 2H); ^{13}C NMR (100 MHz,$CDCl_3$) δ 24.26, 36.26, 49.99, 55.28, 71.93, 114.04, 114.47, 114.68, 127.55, 127.62, 128.78, 128.84, 129.68, 130.31, 139.51, 142.15, 160.51, 163.03. HRMS (ESI) calcd for $C_{23}H_{24}NO_4FS$ $(M + Na)^+$, 452.1308; found, 452.1301.

N-(4-(4-Fluorophenyl)-4-oxobutyl)-4-methoxybenzenesulfonamide (3)

A solution of sodium azide (1.06 g, 16.24 mmol), **20** (1.3 mL, 8.12 mmol), and potassium iodide (134 mg, 0.81 mmol) in DMF (30 mL) was stirred at 90 °C for 8 h. The mixture was diluted with ethyl acetate and water, and separated. The combined organic layers were dried over magnesium sulfate and concentrated in vacuum. The residue **21** was used in the next step without further purification.

A solution of **21** (2 g, 9.65 mmol) and palladium on active charcoal (0.21 g, 0.97 mmol) in MeOH (10 mL) was stirred at room temperature under an atmosphere of hydrogen (1 bar) for 8 h. The mixture was then filtered to form a methanol solution of amine **22**. A mixture of 4-methoxybenzenesulfonyl chloride (2.19 g, 10.62 mmol), triethylamine (2.94 mL, 21.12 mmol) and dry THF (50 mL) was added to the solution of the amine **22** in MeOH. The mixture was stirred for 8 h at 60 °C, extracted with water and ethyl acetate, and separated. The organic layer was dried over magnesium sulfate and concentrated in vacuum. The residue was subjected to flash column chromatography, followed by normal-phase HPLC to afford pure **3** as a white solid (48%): mp 84−85 °C. ^{1}H NMR (400 MHz, acetone-d_6) δ 1.85-1.92 (m, 2H), 3.00-3.03(m, 2H), 3.05-3.10 (m,

2H), 3.88 (s, 3H), 6.39 (t, J = 5.6 Hz, 1H), 7.08 (d, J = 8.8 Hz, 2H), 7.24-7.28 (m, 2H), 7.80 (d, J = 8.8 Hz, 2H), 8.02-8.06 (m, 2H); ^{13}C NMR (100 MHz, acetone-d_6) δ 23. 1, 34.9, 42.4, 55.2, 114.1, 115.4 (d, J = 22 Hz), 128.9, 130.7 (d, J = 9 Hz), 132.8, 133.7, 162.7, 165.5 (d, J = 250 Hz), 197.3. HRMS (ESI) calcd for $C_{17}H_{18}NO_4FS$ $(M + Na)^+$, 374.0838; found, 374.0843.

***N*-(4-(4-Fluorophenyl)-4-oxobutyl)-4-methoxy-N-methylbenzenesulfonamide (4)**

A solution of paraformaldehyde (0.23 g, 7.64 mmol), **22** (1 g, 5.46 mmol), and sodium methoxide (1.47 g, 27.30 mmol) in MeOH (30 mL) was stirred at 90 °C for 4 h, and then cooled to room temperature. Sodium borohydride (0.41 g, 10.92 mmol) was slowly added to the mixture over a 5 min period. The was diluted with ethyl acetate and water, and separated. The organic layer was dried over magnesium sulfate, concentrated in vacuum, giving a residue that was subjected to flash column chromatography to give **23** (0.67 g, 63%).

A solution of 4-methoxybenzenesulfonyl chloride (1.05 g, 5.12 mmol), triethylamine (1.43 mL, 10.24 mmol) and **23** (1.0 g, 5.12 mmol) in THF (20 mL) was stirred at 60 °C for 8 h. The mixture was diluted with ethyl acetate and water, and separated. The organic layer was dried over magnesium sulfate, and concentrated in vacuum. The residue was subjected to flash column chromatography, followed by normal-phase HPLC to afford the pure **4** as a white solid (1.46 g, 78%): mp 89−90 °C. ^{1}H NMR (500 MHz, $CDCl_3$) δ 1.90-1.96 (m, 2H), 2.67 (s, 3H), 3.01-3.05 (m, 4H), 3.81 (s, 3H), 6.91-6.94 (m, 2H), 7.06-7.10 (m, 2H), 7.64-7.67 (m, 2H), 7.93-7.97 (m, 2H); ^{13}C NMR (125 MHz,$CDCl_3$) δ 21.5, 34.7, 35.0, 49.4, 55.6, 114.2, 115.7 (d, J = 22 Hz), 129.0, 129.4, 130.7 (d, J = 9 Hz),

133.3, 162.8, 164.7 (d, J = 254 Hz), 197.9. HRMS (ESI) calcd for $C_{18}H_{20}FNO_4S$ (M + Na)$^+$, 388.0995; found, 388.0995.

General Procedures for Synthesis of Compounds 5−16

To a mixture of sodium hydride (2.52 g, 65.71 mmol) in THF (100 mL) was added amine **24** (5 mL, 54.76 mmol) dropwise over 30 min. The mixture was stirred at 90 ^{o}C for 1 h, followed by the addition of butyrolactone (4.17 mL, 54.76 mmol) dropwise over 10 min. After stirring for 8 h, the mixture was diluted with ethyl acetate and water, and separated. The organic layer was dried over magnesium sulfate, and concentrated in vacuum. The residue was subjected to flash column chromatography to give amide **28** (8.83 g, 90%) as a white solid.

A mixture of lithium aluminum hydride (2.12 g, 55.84 mmol) in THF (100 mL) was added compound **28** (4.0 g, 22.35 mmol) in THF (50 mL) dropwise over 30 min at 0 ^{o}C under argon. The mixture was then stirred at 90 ^{o}C for 8 h, and diluted ethyl acetate and water, and separated. The organic layer was dried over magnesium sulfate, and concentrated in vacuum, giving secondary amine **32**, which was directly used in next step.

A solution of 4-methoxybenzenesulfonyl chloride (4.94 g, 23.99 mmol), triethylamine (5.57 mL, 39.98 mmol), and alcohol **32** (3.30 g, 19.99 mmol) in THF (60 mL) was stirred at 60 ^{o}C for 8 h. The mixture was diluted with ethyl acetate and water, and separated. The organic layer was dried over magnesium sulfate, and concentrated in vacuum. The residue was subjected to flash column chromatography to give amide **36** (5.09 g, 76%).

A mixture of 4 Å molecular sieves (ca. 3.00 g) and pyridinium dichromate (5.09 g, 13.47 mmol) was added to a solution of sulfonyl-amide **36** (3.00 g, 8.98 mmol) in DCM.

The mixture was stirred for 8 h at room temperature, diluted with ethyl acetate and water, and separated. The organic layer was dried over magnesium sulfate, and concentrated in vacuum. The residue was subjected to flash column chromatography to afford the aldehyde **43** (1.95 g, 65%) as a colorless solid.

A solution of methyl iodide (0.42 mL, 6.75 mmol) and magnesium (131 mg, 5.40 mmol) in THF (10 mL) was stirred at 60 ^{o}C for 1 h, and cooled to room temperature. To the mixture was added aldehyde **43** (0.45 g, 1.36 mmol) in THF (10 mL) dropwise over 10 min. After stirring for 2 h, the mixture was diluted with ethyl acetate and water, and separated. The organic layer was dried over magnesium sulfate, and concentrated in vacuum to give secondary alcohol **50**, which was directly used in next step.

A mixture of 4 Å molecular sieves (ca. 1.00 g) and pyridinium dichromate (764 mg, 2.03 mmol) was added to a solution of alcohol **50** in dry DCM (30 mL). The mixture was stirred for 8 h at room temperature, and diluted with ethyl acetate and water, and separated. The organic layer was dried over magnesium sulfate, and concentrated in vacuum. The residue was subjected to flash column chromatography, followed by normal-phase HPLC to afford pure **5** (0.28 g, 60%).

4-Methoxy-*N*-(4-oxopentyl)-*N*-phenylbenzenesulfonamide (5).

Yield 33% (a white solid), mp 81−82 °C. ^{1}H NMR (500 MHz, $CDCl_3$) δ 1.60-1.62 (m, 2H), 2.08 (s, 3H), 2.54 (t, J = 7 Hz, 2H), 3.49 (t, J = 6.5 Hz, 2H), 3.807 (s, 3H), 6.85-6.86 (m, 2H), 6.99 (d, J = 7 Hz, 2H), 7.24-7.26 (m, 3H), 7.44 (d, J = 7 Hz, 2H); ^{13}C NMR (125 MHz,$CDCl_3$) δ 21.8, 30.1, 39.8, 49.5, 55.6, 113.9, 127.9, 128.7, 129.1, 129.7, 139.0, 162.9, 208.1. HRMS (ESI) calcd for $C_{18}H_{21}NO_4S$ $(M + Na)^+$, 370.1089; found, 370.1084.

***N*-(4-Cyclohexyl-4-oxobutyl)-4-methoxy-*N*-phenylbenzenesulfonamide (6).**

Yield 32% (a white solid), mp 81−82 °C. ^{1}H NMR (500 MHz, $CDCl_3$) δ 1.30-1.35 (m, 4H), 1.66-1.68 (m, 4H), 1.70-1.86 (m, 4H), 2.35 (m, 1H), 2.61 (t, *J* = 7 Hz, 2H), 3.57 (t, *J* = 7 Hz, 2H), 3.90 (s, 3H), 6.94 (d, *J* = 8.5 Hz, 2H), 7.07-7.09 (m, 2H), 7.32-7.35 (m, 3H), 7.52 (d, *J* = 8.5 Hz, 2H); ^{13}C NMR (125 MHz,$CDCl_3$) δ 21.8, 25.7, 25.7, 25.8, 28.5, 28.5, 36.8, 49.6, 50.8, 55.6, 113.9, 127.9, 128.7, 129.0, 129.7, 129.8, 139.0, 162.9. HRMS (ESI) calcd for $C_{18}H_{20}FNO_4S$ $(M + Na)^+$, 438.1715 ; found, 438.1710.

***N*-(4-Cyclobutyl-4-oxobutyl)-4-methoxy-*N*-phenylbenzenesulfonamide (7).**

Yield 32% (a gray viscous liquid). ^{1}H NMR (400 MHz, $CDCl_3$) δ 1.61-1.67 (m, 2H), 1.73-1.80 (m, 1H), 1.89-1.98 (m, 1H), 2.05-2.21 (m, 4H), 2.45 (t, *J* = 6.8 Hz, 2H), 3.16-3.23 (m, 1H), 3.51 (t, *J* = 6.8 Hz, 2H), 3.83 (s, 3H), 6.86-6.99 (m, 2H), 7.00-7.02 (d, *J* = 8 Hz, 2H), 7.26-7.28 (m, 3H), 7.45 (d, *J* = 8 Hz, 2H); ^{13}C NMR (100 MHz,$CDCl_3$) δ 22.1, 26.1, 19.1, 49.7, 51.6, 55.7, 114.0, 128.0, 128.8, 128.9, 129.1, 129.9, 129.9, 139.2, 163.0, 212.7. HRMS (ESI) calcd for $C_{21}H_{25}NO_4S$ $(M + Na)^+$, 410.1402; found, 410.1407.

***N*-(4-Cyclopentyl-4-oxobutyl)-4-methoxy-*N*-phenylbenzenesulfonamide (8).**

Yield 35% (a white solid), mp 89−90 °C. ^{1}H NMR (400 MHz, $CDCl_3$) δ 1.60-1.79 (m, 10H), 2.53 (t, *J* = 7.2 Hz, 2H), 2.75-2.83 (m, 1H), 3.49 (t, *J* = 6.4 Hz, 2H), 3.80 (s, 3H), 6.84-6.87 (m, 2H), 6.98-7.01 (m, 2H), 7.22-7.26 (m, 3H), 7.43 (d, *J* = 8.8 Hz, 2H); ^{13}C NMR (100 MHz, $CDCl_3$) δ 22.1, 26.1, 26.1, 29.1, 29.1, 38.1, 49.8, 51.7, 55.7, 114.1, 128.1, 128.9, 129.0, 129.2, 129.9, 139.2, 163.0, 212.7. HRMS (ESI) calcd for $C_{22}H_{27}NO_4S$ $(M + Na)^+$, 424.1559; found, 424.1552.

***N*-(4-Cycloheptyl-4-oxobutyl)-4-methoxy-*N*-phenylbenzenesulfonamide (9).**

Yield 34% (a white solid), mp 75−76 °C. ^{1}H NMR (400 MHz, $CDCl_3$) δ 1.42-1.80 (m, 14H), 2.43-2.56 (m, 1H), 2.55 (t, *J* = 7.2 Hz, 2H), 3.51 (m, *J* = 6.4 Hz, 2H), 3.83 (s, 3H),

6.87 (d, J = 8.8 Hz, 2H), 7.00-7.03 (m, 2H), 7.27-7.28 (m, 3H), 7.45 (d, J = 8.8 Hz, 2H); ^{13}C NMR (100 Hz, $CDCl_3$) δ 22.2, 26.9, 26.9, 28.5, 28.5, 30.1, 30.1, 37.2, 49.8, 52.6, 55.8, 114.1, 128.1, 128. 9, 129.2, 130.0, 139.3, 163.1, 213.9. HRMS (ESI) calcd for $C_{24}H_{31}NO_4S$ $(M + Na)^+$, 452.1872; found, 452.1866.

N-(4-(Adamantan-2-yl)-4-oxobutyl)-4-methoxy-N-phenylbenzenesulfonamide (10).

Yield 35% (a white solid), mp 117−118 °C. ^{1}H NMR (400 MHz, $CDCl_3$) δ 1.54-1.88 (m, 14H), 2.3 (s, 2H), 2.41 (s, 1H), 2.53 (t, J = 7 Hz, 2H), 3.52 (t, J = 6.4 Hz, 2H), 3.83 (s, 3H), 6.86-6.89 (m, 2H), 7.00-7.02 (m, 2H), 7.26-7.28 (m, 3H), 7.45 (d, J = 8.8 Hz, 2H); ^{13}C NMR (100 Hz, $CDCl_3$) δ 22.2, 27.7, 27.8, 29.4, 29.4, 33.5, 33.5, 36.2, 37.5, 38.5, 38.5, 49.8, 55.8, 57.3, 114.1, 128.1, 128.9, 129.2, 129.9, 139.2, 163.0, 212. 3. HRMS (ESI) calcd for $C_{27}H_{33}NO_4S$ $(M + Na)^+$, 490.2028; found, 490.2033.

N-(4-Cyclopentyl-4-oxobutyl)-N-phenyl-4-(trifluoromethoxy)benzenesulfonamide (11).

Yield 32% (a white solid), mp 69−70 °C. ^{1}H NMR (400 MHz, $CDCl_3$) δ 1.56-1.77 (m, 8H), 1.79-1.82 (m, 2H), 2.56 (t, J = 7.2 Hz, 2H), 2.78-2.86 (m, 1H), 3.56 (t, J = 6.4 Hz, 2H), 7.00-7.03 (m, 2H), 7.23-7.25 (m, 2H), 7.29-7.31 (m, 3H), 7.57-7.59 (m, 2H); ^{13}C NMR (100 Hz, $CDCl_3$) δ 22.2, 26.2, 26.2, 29.1, 38.1, 50.0, 51.7, 120.8, 128.5,128.8, 129.5, 129.9, 136.7, 138.7, 152.3, 212.6 HRMS (ESI) calcd for $C_{22}H_{25}NO_4SF_3$ $(M + H)^+$, 456.1456; found, 456.1458.

N-(4-Cycloheptyl-4-oxobutyl)-4-phenoxy-N-phenylbenzenesulfonamide (12).

Yield 35% (a white solid), mp 127−128 °C. ^{1}H NMR (400 MHz, $CDCl_3$) δ 1.40-1.80 (m, 14H), 2.45-2.49 (m, 1H), 2.55 (t, J = 7.2 Hz, 2H), 3.53 (t, J = 6.4 Hz, 2H), 6.93-6.95 (m, 2H), 7.03-7.05 (m, , 4H), 7.18-7.30 (m, 4H), 7.37-7.41 (m, , 2H), 7.46-7.48 (m, 2H); ^{13}C

NMR (100 Hz, $CDCl_3$) δ 22.0, 26.6, 28.3, 29.9,37.0, 49.6, 52.4, 117.3, 120.3, 125.0, 128.0,128.6, 129.0, 129.8, 130.2, 131.8, 139.0, 155.2, 162.5, 213.7. HRMS (ESI) calcd for $C_{29}H_{33}NO_4S$ $(M + Na)^+$, 514.2028; found, 514.2023.

_N_-(5-Cycloheptyl-5-oxopentyl)-4-methyl-_N_-phenylbenzenesulfonamide (13).

Yield 23% (a gray viscous liquid). ^1H NMR (300 MHz, $CDCl_3$) δ 1.56-1.86 (m, 16H), 2.46 (s, 3H), 2.59.2.64 (m, 1H), 2.62 (t, J = 6.6 Hz, 2H), 3.58 (t, J = 6.45 Hz, 2H), 7.06-7.09 (m, 2H), 7.26-7.35 (m, 5H), 7.42 (d, J = 8.4 Hz, 2H); ^{13}C NMR (75 Hz, $CDCl_3$) δ 21.7, 22.2, 26.7, 26.7, 28.5, 28.5, 30.2, 30.2, 37.2, 49.9, 52.7, 127.9, 128.1, 129.0, 129.3, 129.6, 135.4, 139.2, 143.6, 214.0. HRMS (ESI) calcd for $C_{24}H_{33}NO_4S$ $(M + Na)^+$, 436.1922; found, 436.1917.

_N_-(4-Cycloheptyl-4-oxobutyl)-_N_-cyclohexyl-4-methoxybenzenesulfonamide (14).

Yield 32% (a gray viscous liquid). ^1H NMR (400 MHz, $CDCl_3$) δ 1.32-1.86 (m, 23H), 2.49 (t, J = 7 Hz, 2H), 3.07-3.11 (m, 2H), 3.50-3.56 (m, 1H), 3.82 (s, 3H), 6.90 (d, J = 8, 2H), 7.69 (t, J = 4.4 Hz, 2H); ^{13}C NMR (100 MHz,$CDCl_3$) δ 25.5, 26.0, 26.3, 26.3, 26.9, 26.9, 28.5, 28.5, 30.2, 30.2, 31.9, 31.9, 37.9, 43.3, 52.5, 55.7, 58.2, 114.3, 129.1, 162.7, 214.2. HRMS (ESI) calcd for $C_{24}H_{33}NO_3S$ $(M + Na)^+$, 458.2341; found, 458.2346.

N-(4-cycloheptyl-4-oxobutyl)-4-methoxy-N-(5,6,7,8-tetrahydronaphthalen-2-yl)benzenesulfonamide (15).

Yield 32% (a white solid), mp 111−112 °C. ^1H NMR (300 MHz, $CDCl_3$) δ 144-1.82 (m, 20H), 2.50-2.55 (m, 3H), 2.78-2.98 (m, 3H), 3.15-3.24 (m, 1H), 3.60-3.70 (m, 1H), 3.87 (s, 3H), 6.38-6.41 (m, 1H), 6.92-6.97 (m, 4H), 7.58 (d, 2H); ^{13}C NMR (75 MHz,$CDCl_3$) δ 22.5, 22.9, 22.9, 26.0, 26.0, 26.9, 26.9, 28.5, 29.9, 30.1, 30.2, 37.8, 51.5, 52.6, 55.8,114.1,

125.2, 125.6, 129.5, 130.3, 130.8, 138.4, 139.5, 139.6, 163.1, 213.7. HRMS (ESI) calcd for $C_{30}H_{41}NO_4S$ $(M + Na)^+$, 506.2341; found, 506.2332.

N-(4-cycloheptyl-4-oxobutyl)-N-(4-cyclohexylphenyl)-4-methoxybenzenesulfonamide (16).

Yield 35% (a white solid), mp 103−104 °C. ^{1}H NMR (300 MHz, $CDCl_3$) δ 1.51-1.85 (m, 24H), 2.43-2.49 (m, 2H), 2.55 (t, *J* = 7.2 Hz, 2H), 3.47 (t, *J* = 6.6 Hz, 2H), 3.83 (s, 3H), 6.86-6.92 (m, 4H), 7.09 (d, *J* = 8.4 Hz, 2H), 7.47 (d, *J* = 8.7 Hz, 2H); ^{13}C NMR (75 MHz,$CDCl_3$) 22.2, 26.2, 26.8, 26.8, 26.9, 26.9, 28.4, 28.4, 30.1, 30.1, 34.5, 34.5, 37.2, 44.2, 49.9, 52.5, 55.7, 114.0, 127.5, 128.3, 129.9, 130.2, 136.7, 148.0, 162.9, 214.0. HRMS (ESI) calcd for $C_{30}H_{41}NO_4S$ $(M + Na)^+$, 534.2654; found, 534.2648.

Construction of DENV-2-eGFP reporter virus

The DENV-2 infectious clone with the SP6 promoter (SP6-Den2) was prepared as follows. The RNA of DENV-2 PL046 strain (Genbank accession: AJ968413.1) was extracted and subjected to the reverse transcription polymerase chain reaction (RT-PCR) to produce 5 cDNA fragments (nucleotide region: 1-1512, 1342-4250, 4132-6375, 4522-9368, and 6838-10723), which were subsequently cloned into the polylinker of pJET1.2. The full-length viral cDNA clone was then generated by using the vector pBR322 and the standard restriction enzyme and ligation strategy. To construct the DENV-2-eGFP reporter virus, eGFP-2A containing eGFP and the porcine teschovirus (PTV1) 2A sequences, was inserted into SP6-Den2 between 5′ UTR and the DENV-2 ATG start codon. The DENV-2 cyclization sequence was silently mutated by single primer PCR mutagenesis. Sequences encoding the first 34 amino acids of DENV-2 capsid protein and the cyclization sequence were inserted into the SP6-Den2 infectious clone by using PCR and blunt end ligation.

Viral RNA of the reporter DENV-2 was transcribed from the SP6 promoter *in vitro*. Production of reporter DENV-2 was carried out by transfection of viral RNA into baby hamster kidney BHK-21 cells (ATCC: CCL-10) using Lipofectamine 2000. Amplification of the reporter virus was carried out with mosquito C6/36 cells (ATCC: CRL-1660).

Cell lines and cell-based anti-DENV-2 screening

Human neuroblastoma BE(2)C cells (ATCC: CRL-2268) were cultured in RPMI 1640 medium (Gibco) supplemented with 10% fetal bovine serum (FBS). Human microglia HMC3 cells (ATCC: CRL-3304) were grown in MEM (HyClone) containing 10% FBS. BE(2)C cells were plated using a black 96-wells plate with a clear flat bottom (Corning Costar 3603). Cells were infected with DENV-2-eGFP reporter virus (Multiplicity of infection [MOI], 1) for 24 h, in the absence or presence of the test compound at the specified concentration. DMSO was used as the solvent control. Cells were fixed with 4% paraformaldehyde, and then stained with Hoechst for nuclei. The antiviral activity of the test compounds was evaluated by measuring the intensity of eGFP with the ImageXpress Micro XLS High-Content Analysis System (Molecular Devices). The relative intensity of eGFP to cell number of treated cells is reported as the percentage of the solvent control.

Cytotoxicity assays

The cytotoxicity of the test compounds towards BE(2)C and HMC3 cells was evaluated by use of the Cytotoxicity Detection Kit (LDH) (Roche), Cell Proliferation Kit (XTT) (Roche), and Trypan blue cell counting assay. Briefly, cells were treated with the indicated doses of the test compound overnight and then subjected to the cytotoxicity assays. Sample absorbances were measured at 490 nm for the XTT and LDH assays by

using an ELISA reader (Molecular Devices). Trypan blue cell counting assay was used to determine the viable cell number. The values were normalized by calculating the percent of the solvent control.

Antiviral assays of 9

The DENV-2 PL046 strain (Genbank accession: AJ968413.1) isolated from a Taiwan dengue fever patient[40] and the ZIKV PRVABC59 strain (Genbank accession: KU501215) provided by the Centers for Disease Control, Taiwan, were used for *in vitro* studies. BE(2)C and HMC3 cells were infected for 48 h with DENV-2 or ZIKV (MOI, 0.1) in the absence or presence of **9**, at the specified concentrations. The antiviral activity of **9** was evaluated by immunoblotting (WB) and by using the immunofluorescence assay (IFA) and the plaque-forming assay (PFA). The expression of the proteins DENV-2-NS3 and ZIKV-E was detected in cells with the respective antibodies anti-DENV-NS3[40] and anti-flavivirus E[41]. Alexa Fluor-488-conjugated anti-mouse secondary antibody (Molecular Probes) and Hoechst stain (Molecular Probes) for nuclei staining were used in the IFA. Cells were examined under an inverted fluorescence microscope (Olympus 1X71). Anti-β-actin (Chemicon) and horseradish peroxidase (HRP)-conjugated secondary antibody (Jackson ImmunoResearch) were used for the WB; signals were detected by enhanced chemiluminescence (ECL, Pierce). The level of infectious DENV-2 and ZIKV was measured by PFA in BHK-21 (ATCC: CCL-10) and Vero (ATCC: CRL-1587) cells, respectively[42]. The virus titer was determined as Log plaque-forming unit (PFU)/mL and used to access the half-maximal effective concentration (EC_{50}). The EC_{50} was calculated according to published procedure [43]. In addition, the antiviral activity of **9** against human influenza A (H1N1) virus and recombinant sindbis virus expressing eGFP (dSinF-

EGFP/2A)[44] were performed. The expression of influenza A nucleoprotein (NP) (GeneTex, GTX125989) and eGFP-positive cells were evaluated by immunofluorescence microscopy.

Virus binding and entry assays

Virus binding and entry assays were performed as described previously[13]. For virus binding assay, cells were incubated with DENV-2 or ZIKV for 90 min at 4 °C, with rocking on linear shaker, in the absence or presence of **9**. For the virus entry assay, cells were incubated with DENV-2 or ZIKV for 90 min at 4 °C. After a gentle wash with cold medium, the cells were treated with **9** at the specified concentrations and then incubated at 37 °C for 1 h to allow virus entry. The cells were then treated with glycine (0.1 M, pH = 3) for 5 min to inactivate non-internalized virus prior to washing with cold HBSS. Cells were harvested with use of cell scrapers, and the adsorbed viruses were released by passing the cells through a 27-G needle 7 times. Cell lysates were centrifuged at 12,000 rpm for 1 min, and the supernatant was used for the plaque-forming assay.

Fluorescently labeled virus and confocal imaging

DENV-2 and ZIKV were concentrated by ultracentrifugation at 47,000 rpm and 4 ^{o}C for 4 h using a Beckman 50.2 Ti rotor. The viral pellets were re-suspended in 1 mL of HNE buffer (5 mM HEPES, 150 mM NaCl, 0.1 mM EDTA, pH 7.4) and labeled using atto-647N-NHS ester fluorescence dye. Subsequently, the atto 647N-labeled viral particles were purified using Sephadex G-25 contained in a PD-10 desalting column (GE, Catalog No. 17085101). The level of virus titer was determined by using the plaque-forming assay. Fluorescently labeled viruses were used for confocal microscopy imaging in order to evaluate the effect of **9** on viral entry. Briefly, viral entry assays were performed with

BE(2)C cells first treated with solvent or 3.125 μM **9**, and then incubated at 37 °C with DENV-2 for 30 min or with ZIKV for 60 min. Next, the cells were washed with PBS and fixed with 4% paraformaldehyde for 15 min at room temperature. After washing with PBS, the cell membranes were stained with WGA-488. Images were acquired by the use of a confocal microscope (Olympus®, FluoView 1000 confocal microscope equipped with 100×, oil, NA1.4 objective lens).

Animal study

The mouse experiments were conducted according to the guideline outlined by Council of Agriculture Executive Yuan, Republic of China. This animal protocol was approved by the Academia Sinica Institutional Animal Care and Use Committee (Protocol no. 14-10-743) and was performed in accordance with the guidelines. Infection was performed in mice under isoflurane anesthesia and efforts were made to minimize animal suffering.

The DENV-2 New Guinea C strain serially passaged in mouse brain (NGC-N) (kindly provided by Dr. Ching-Juh Lai, National Institutes of Health, USA) and the ZIKV PRVABC59 strain (Genbank accession: KU501215) were used in the animal study. Groups of 6-week-old Stat1$^{-/-}$ mice were intravenously infected in the tail with 1x10^5 PFU of DENV-2 (NGC-N) per mouse or subcutaneously infected in the footpad with 5x10^4 PFU of ZIKV (PRVABC59) per mouse. To study the efficacy of **9** administered by an oral route, mice were divided into several groups for treatment: phosphate buffered saline (PBS; vehicle control) and 2, 4, or 8 mg of **9**/kg body weight/mouse/oral/day at the time of infection (immediate treatment) or at 8 h post-infection (8 h-delay treatment) up to day 6 after infection. The mice were checked daily for symptoms including limb paralysis.

Euthanasia of mice with severe limb paralysis was performed as the endpoint of animal survival. Serum samples were collected on day 3 after infection by phlebotomy from the facial vein (submandibular) and the virus load was determined by using the plaque-forming assay.

Computational docking analysis

Molecular docking studies were carried out with CaMKIIα (PDB accession code 2VZ6) and other kinases including Axl (PDB accession code 5U6B), Tyro3 (PDB accession code 2QUP), and p38MAPK (PDB accession code 5XYX) by the use of SwissDock[45]. Briefly, Indirubin E804 and non-polar hydrogen atoms were removed from the structure of CaMKIIα. Polar hydrogen atoms were added to the structure, and used as the drug target protein. Structure of **9** for docking was generated with ChemSketch (ACD Inc)[46]. An accurate docking analysis was selected to predict the interaction between tested compounds and kinases. Free energy binding was calculated using molecular mechanics energies with the Poisson-Boltzmann (MM/PBSA) that takes into account bonded and van der Waals interaction as well as polar and non-polar contributions[47]. Docked structures were visualized with UCSF chimera[48].

CaMKII biochemical assay

The inhibitory effect of **9** on purified human CaMKIIα was accessed by using an immunoassay carried out according to manufacturer's instructions (CycLex CaM kinase II Assay Kit, MBL Intl Corp). Briefly, CaMKIIα activity was measured in the absence and presence of **2**, **3**, **8**, **9**, or **16** using microtiter plates to contain the reactions solutions composed of 2 mM $CaCl_2$, 5 mM $MgCl_2$, 100 μM ATP, 200 ng calmodulin, 4 μg syntide-2 and 20 mM Hepes KOH (pH 4.5) at 30^{o}C for 30 minutes. The kinase buffer was added

first to the wells, followed by incubation with HRP-conjugated-anti-phospho-syntide-2 antibody. Subsequently, the reaction components were added and following incubation for 15 min at room temperature, the absorbance of the reaction solution at 450 nm was determined with an ELISA reader (Molecular Devices). Three types of control reactions were carried out, one which included DMSO (solvent control), one which included the commercially available CaMKII inhibitor KN-62 (Selleckchem, S7422, IC_{50} = 0.9 μM) (positive control) and one which excluded Ca^{2+} (negative control). Each reaction rate was reported as the percentage of that of the solvent control.

Lentivirus preparation and CaMKII knockdown

The lentivirus vector which carries a pool of short hairpin RNA (shRNA) targeting the human CaMKIIα (Santa Cruz, SC-29900-SH) or LacZ (5′-TGTTCGCATTATCCGAACCAT-3′, TRCN0000072223. Taiwan National RNAi Core Facility) was cotransfected with pMD.G and pCMVΔR8.91 into HEK293T cells by use of Lipofectamine 2000 (Invitrogen). The lentiviruses were harvested from culture supernatants and used to transduce BE(2)C cells. CaMKIIα-deficient BE(2)C cells (shCaMKIIα-BE(2)C) and LacZ-control cells (shLacZ-BE(2)C) were selected with puromycin (10 μg/mL). Antibodies for phosphorylated-CaMKIIα (Thermo Scientific, 22B1) and CaMKII (Invitrogen, PA5-99558) were used in immunofluorescence and Western blot analysis.

Statistical analysis

Data are reported as the mean ± standard deviation and were compared by ANOVA and Bonferroni post-hoc test. Statistical significance was set at P values of < 0.05 (*) and < 0.01 (**). The survival curve was analyzed with SigmaPlot v10.0 (Systat software).

Determination of the median survival time (T_{50}) and *P* values, by the log-rank test, involved use of Prism v5.0 (GraphPad software). For analysis of the immunoblots, the band densities were quantified by using ImageJ software (National Institute of Health).

ASSOCIATED CONTENT

Supporting Information. The Supporting Information is available free of charge via the Internet at **http://pubs.acs.org**.

Determination of the cytotoxicity and antiviral activity of **9** against DENV-2 and ZIKV infection (multiplicity of infection [MOI], 1) in human microglial HMC3 cells; antiviral activity of **9** against influenza H1N1 and Sindbis (SINV) virus infection; molecular docking of BSA-kinases and the estimated binding free energy (MM/PBSA); biochemical assay of BSA **2**, **3**, **8**, and **16** on human CaMKIIIα activity by use of CycLex CaM Kinase II assay. Details of HPLC-determined purity data, high-resolution mass spectrometry results, 1 H and 13C NMR spectra of all new benzenesulfonamide (BSA) derivatives.

Molecular formula strings and some data.

AUTHOR INFORMATION

Corresponding Author

*Correspondence: Yogy Simanjuntak, Ph.D., yogy@ibms.sinica.edu.tw; Yi-Ling Lin, Ph.D., yll@ibms.sinica.edu.tw; Wen-Shan Li, Ph.D., wenshan@gate.sinica.edu.tw.

ORCID

Yogy Simanjuntak: 0000-0002-8983-0451

Yueh-Hsin Ping: 0000-0003-2604-9913

Yi-Ling Lin: 0000-0002-1838-6410

Wen-Shan Li: 0000-0002-8359-4582

Author contributions

WCC and YS designed and synthesized the compounds, performed research, and analyzed data. LWC and YHP performed confocal microscopy experiments. YL Lee provided critical reagents. YS, YL Lin, and WSL conceptualized the research, and wrote and edited the manuscript.

[#]These authors, Wei-Chia Chen and Yogy Simanjuntak, contributed equally as the first author.

ACKNOWLEDGMENT

We thank Taiwan CDC for Zika virus (PRVABC59). We also thank the core facility of Institute of Biomedical Sciences for technical assistance. Instrumentation support was provided by the NMR and Mass Spectrometry facilities of the Institute of Chemistry at Academia Sinica, Taiwan. This study was financially supported by Academia Sinica (AS-SUMMIT-109 and AS-KPQ-109-BioMed) and Ministry of Science and Technology, Taiwan (Grant: MOST 108-3114-Y-001-002, MOST 108-2321-B-001-011, MOST 108-2320-B-001-030-MY3, MOST 108-3111-Y-001-056, MOST 108-2113-M-001-020 and MOST 108-2320-B-010-031).

ABBREVIATIONS

BSA, Benzenesulfonamide; CaMKII, Calcium/calmodulin-dependent kinase II; DENV, Dengue virus, ZIKV, Zika virus; MOI, Multiplicity of infection.

REFERENCES

1. Guzman, M. G.; Halstead, S. B.; Artsob, H.; Buchy, P.; Farrar, J.; Gubler, D. J.; Hunsperger, E.; Kroeger, A.; Margolis, H. S.; Martinez, E.; Nathan, M. B.; Pelegrino, J. L.; Simmons, C.; Yoksan, S.; Peeling, R. W. Dengue: a continuing global threat. *Nat Rev Microbiol* **2010,** 8, S7-16.

2. Bhatt, S.; Gething, P. W.; Brady, O. J.; Messina, J. P.; Farlow, A. W.; Moyes, C. L.; Drake, J. M.; Brownstein, J. S.; Hoen, A. G.; Sankoh, O.; Myers, M. F.; George, D. B.; Jaenisch, T.; Wint, G. R.; Simmons, C. P.; Scott, T. W.; Farrar, J. J.; Hay, S. I. The global distribution and burden of dengue. *Nature* **2013,** 496, 504-7.

3. Gubler, D. J. Epidemic dengue/ dengue hemorrhagic fever as a public health, social and economic problem in the 21st century. *TRENDS in Microbiol* **2002,** 10, 100-103.

4. Petersen, L. R.; Jamieson, D. J.; Powers, A. M.; Honein, M. A. Zika Virus. *N Engl J Med* **2016,** 374, 1552-63.

5. Plourde, A. R.; Bloch, E. M. A Literature Review of Zika Virus. *Emerg Infect Dis* **2016,** 22, 1185-92.

6. Rodenhuis-Zybert, I. A.; Wilschut, J.; Smit, J. M. Dengue virus life cycle: viral and host factors modulating infectivity. *Cell Mol Life Sci* **2010,** 67, 2773-86.

7. Musso, D.; Gubler, D. J. Zika Virus. *Clin Microbiol Rev* **2016,** 29, 487-524.

8. Miner, J. J.; Diamond, M. S. Zika Virus Pathogenesis and Tissue Tropism. *Cell Host Microbe* **2017,** 21, 134-142.

9. Calderon-Pelaez, M. A.; Velandia-Romero, M. L.; Bastidas-Legarda, L. Y.; Beltran, E. O.; Camacho-Ortega, S. J.; Castellanos, J. E. Dengue Virus Infection of Blood-Brain Barrier Cells: Consequences of Severe Disease. *Front Microbiol* **2019,** 10, 1435.

10. Bardina, S. V.; Bunduc, P.; Tripathi, S.; Duehr, J.; Frere, J. J.; Brown, J. A.; Nachbagauer, R.; Foster, G. A.; Krysztof, D.; Tortorella, D.; Stramer, S. L.; Garcia-Sastre, A.; Krammer, F.; Lim, J. K. Enhancement of Zika virus pathogenesis by preexisting antiflavivirus immunity. *Science* **2017,** 356, 175-180.

11. Kawiecki, A. B.; Christofferson, R. C. Zika Virus-Induced Antibody Response Enhances Dengue Virus Serotype 2 Replication In Vitro. *J Infect Dis* **2016,** 214, 1357-1360.

12. Leyssen, P.; De Clercq, E.; Neyts, J. Perspectives for the treatment of infections with flaviviridae. *Clin Microbiol Rev* **2000,** 13, 67-82.

13. Simanjuntak, Y.; Liang, J. J.; Lee, Y. L.; Lin, Y. L. Japanese Encephalitis Virus Exploits Dopamine D2 Receptor-phospholipase C to Target Dopaminergic Human Neuronal Cells. *Front Microbiol* **2017,** 8, 651.

14. Coultrap, S. J.; Bayer, K. U. CaMKII regulation in information processing and storage. *Trends Neurosci* **2012,** 35, 607-18.

15. Ebenebe, O. V.; Heather, A.; Erickson, J. R. CaMKII in Vascular Signalling: "Friend or Foe"? *Heart, Lung and Circulation* **2018,** 27, 560-567.

16. Liu, X.; Zhan, Z.; Xu, L.; Ma, F.; Li, D.; Guo, Z.; Li, N.; Cao, X. MicroRNA-148/152 impair innate response and antigen presentation of TLR-triggered dendritic cells by targeting CaMKIIalpha. *J Immunol* **2010,** 185, 7244-51.

17. Pellicena, P.; Schulman, H. CaMKII inhibitors: from research tools to therapeutic agents. *Front Pharmacol* **2014,** 5, 21.

18. Yang, X.; Wu, N.; Song, L.; Liu, Z. Intrastriatal injections of KN-93 ameliorates levodopa-induced dyskinesia in a rat model of Parkinson's disease. *Neuropsychiatr Dis Treat* **2013,** 9, 1213-20.

19. Sumi, M.; Kiuchi, K.; Ishikawa, T.; Ishii, A.; Hagiwara, M.; Nagatzu, T.; Hidaka, H. The newly sunthesized selective Ca2+/calmodulin dependent kinase II inhibitor KN-93 reduces dopamine contents in PC12h cells. *Biochem Biophys Res Commun* **1991,** 181, 968-975.

20. Boothe, J. R.; Shen, Y.; Wolfe, J. P. Synthesis of Substituted γ-and δ-Lactams via Pd-Catalyzed Alkene Carboamination Reactions. *The Journal of organic chemistry* **2017,** 82, 2777-2786.

21. Feng, Y.; Yu, Z.-X. Formal Synthesis of (±)-Galanthamine and (±)-Lycoramine Using Rh (I)-Catalyzed [(3+ 2)+ 1] Cycloaddition of 1-Ene–Vinylcyclopropane and CO. *The Journal of organic chemistry* **2015,** 80, 1952-1956.

22. Kikue, N.; Takahashi, T.; Nishino, H. Mn (III)-Based Oxidative Cyclization of N-Aryl-3-oxobutanamides. Facile Synthesis and Transformation of Substituted Oxindoles. **2015**.

23. Chen, J.-Q.; Wei, Y.-L.; Xu, G.-Q.; Liang, Y.-M.; Xu, P.-F. Intramolecular 1, 5-H transfer reaction of aryl iodides through visible-light photoredox catalysis: a concise method for the synthesis of natural product scaffolds. *Chemical Communications* **2016,** 52, 6455-6458.

24. Miyamoto, H.; Hirano, T.; Okawa, Y.; Nakazaki, A.; Kobayashi, S. Stereoselective synthesis of spirocyclic oxindoles based on a one-pot Ullmann coupling/Claisen rearrangement and its application to the synthesis of a hexahydropyrrolo [2, 3-b] indole alkaloid. *Tetrahedron* **2013,** 69, 9481-9493.

25. Fournier, D.; Poirier, D. Chemical synthesis and evaluation of 17α-alkylated derivatives of estradiol as inhibitors of steroid sulfatase. *European journal of medicinal chemistry* **2011,** 46, 4227-4237.

26. DeTulleo, L.; T, K. The clathrin endocytic pathway in viral infection. *EMBO J* **1998,** 17, 4585-93.

27. Chen, S. T.; Lin, Y. L.; Huang, M. T.; Wu, M. F.; Cheng, S. C.; Lei, H. Y.; Lee, C. K.; Chiou, T. W.; Wong, C. H.; Hsieh, S. L. CLEC5A is critical for dengue-virus-induced lethal disease. *Nature* **2008,** 453, 672-6.

28. Durbin, J. E.; Hackenmiller, R.; Simon, M. C.; Levy, D. E. Targeted disruption of the mouse Stat1 gene results in compromised innate immunity to viral disease. *Cell* **1996,** 84, 443-50.

29. Saha, S.; Ramanathan, A.; Rangarajan, P. N. Regulation of Ca2+/calmodulin kinase II inhibitor alpha (CaMKIINalpha) in virus-infected mouse brain. *Biochem Biophys Res Commun* **2006,** 350, 444-9.

30. Jin, Y.; Zhang, R.; Wu, W.; Duan, G. Antiviral and Inflammatory Cellular Signaling Associated with Enterovirus 71 Infection. *Viruses* **2018,** 10.

31. Prevarskaya, N.; Skryma, R.; Shuba, Y. Calcium in tumor metastasis: new roles for known actors. *Nat Rev Cancer* **2011,** 11, 609-18.

32. Guzman, M. G.; Wang, J.-L.; Zhang, J.-L.; Chen, W.; Xu, X.-F.; Gao, N.; Fan, D.-Y.; An, J. Roles of Small GTPase Rac1 in the Regulation of Actin Cytoskeleton during Dengue Virus Infection. *PLoS Neglected Tropical Diseases* **2010,** 4.

33. Chu, J. J.; Ng, M. L. Interaction of West Nile virus with alpha v beta 3 integrin mediates virus entry into cells. *J Biol Chem* **2004,** 279, 54533-41.

34. Liang, J. J.; Yu, C. Y.; Liao, C. L.; Lin, Y. L. Vimentin binding is critical for infection by the virulent strain of Japanese encephalitis virus. *Cell Microbiol* **2011,** 13, 1358-70.

35. Rosenberg, O. S.; Deindl, S.; Sung, R. J.; Nairn, A. C.; Kuriyan, J. Structure of the autoinhibited kinase domain of CaMKII and SAXS analysis of the holoenzyme. *Cell* **2005,** 123, 849-60.

36. Yilmaz, M.; Gangopadhyay, S. S.; Leavis, P.; Grabarek, Z.; Morgan, K. G. Phosphorylation at Ser(2)(6) in the ATP-binding site of Ca(2)(+)/calmodulin-dependent kinase II as a mechanism for switching off the kinase activity. *Biosci Rep* **2013,** 33.

37. Bayer, K. U.; LeBel, E.; McDonald, G. L.; O'Leary, H.; Schulman, H.; De Koninck, P. Transition from reversible to persistent binding of CaMKII to postsynaptic sites and NR2B. *J Neurosci* **2006,** 26, 1164-74.

38. Haqshenas, G.; Doerig, C. Targeting of host cell receptor tyrosine kinases by intracellular pathogens. *Sci Signal* **2019,** 12, 1-10.

39. Ceballos-Olvera, I.; Chavez-Salinas, S.; Medina, F.; Ludert, J. E.; del Angel, R. M. JNK phosphorylation, induced during dengue virus infection, is important for viral infection and requires the presence of cholesterol. *Virology* **2010,** 396, 30-6.

40. Lin, Y. L.; Liao, C. L.; Chen, L. K.; Yeh, C. T.; Liu, C. I.; Ma, S. H.; Huang, Y. Y.; Huang, Y. Y.; Kao, C. L.; King, C. C. Study on dengue virus infection in SCID mice engrafted with human K562 cells. *J Virol* **1998,** 72, 9729-9737.

41. Simanjuntak, Y.; Liang, J. J.; Chen, S. Y.; Li, J. K.; Lee, Y. L.; Wu, H. C.; Lin, Y. L. Ebselen alleviates testicular pathology in mice with Zika virus infection and prevents its sexual transmission. *PLoS Pathog* **2018,** 14, e1006854.

42. Agbulos, D. S.; Barelli, L.; Giordano, B. V.; Hunter, F. F. Zika Virus: Quantification, Propagation, Detection, and Storage. *Curr Protoc Microbiol* **2016,** 43, 15D 4 1-15D 4 16.

43. Alexander, B.; Browse, D. J.; Reading, S. J.; Benjamin, I. S. A simple and accurate mathematical method for calculation of the EC50. *J Pharmacol Toxicol* **1999,** 41, 55-58.

44. Lin, R. J.; Chien, H. L.; Lin, S. Y.; Chang, B. L.; Yu, H. P.; Tang, W. C.; Lin, Y. L. MCPIP1 ribonuclease exhibits broad-spectrum antiviral effects through viral RNA binding and degradation. *Nucleic Acids Res* **2013,** 41, 3314-26.

45. Grosdidier, A.; Zoete, V.; Michielin, O. SwissDock, a protein-small molecule docking web service based on EADock DSS. *Nucleic Acids Res* **2011,** 39, W270-7.

46. Hunter, A. D. ACD/ChemSketch 1.0 (freeware); ACD/ChemSketch 2.0 and its Tautomers, Dictionary, and 3D Plug-ins; ACD/HNMR 2.0; ACD/CNMR 2.0. *J Chem Educ* **1997,** 74, 905.

47. Genheden, S.; Ryde, U. The MM/PBSA and MM/GBSA methods to estimate ligand-binding affinities. *Expert Opin Drug Discov* **2015,** 10, 449-61.

48. Pettersen, E. F.; Goddard, T. D.; Huang, C. C.; Couch, G. S.; Greenblatt, D. M.; Meng, E. C.; Ferrin, T. E. UCSF Chimera--a visualization system for exploratory research and analysis. *J Comput Chem* **2004,** 25, 1605-12.

TOC

CaMKII inhibitors inhibited viral entry and suppressed DENV-2 and ZIKV infections in the mouse challenge models.

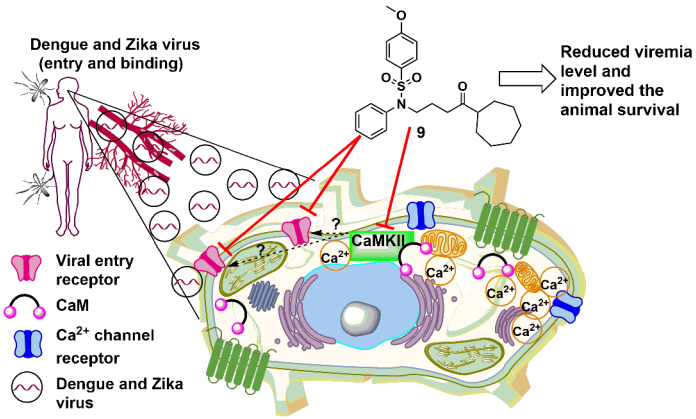

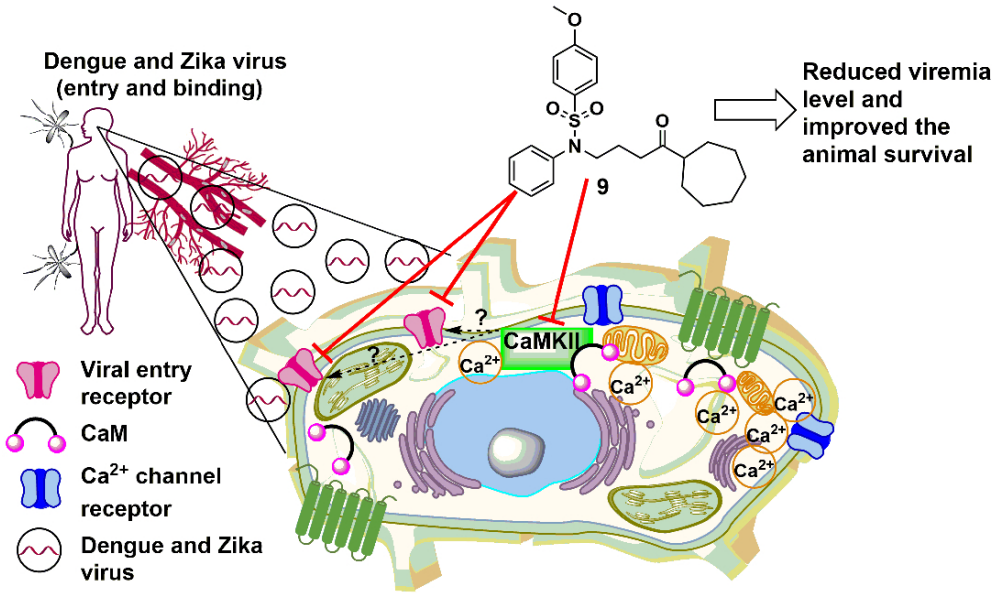

TOC: CaMKII inhibitors inhibited viral entry and suppressed DENV-2 and ZIKV infections in the mouse challenge models.

92x55mm (300 x 300 DPI)

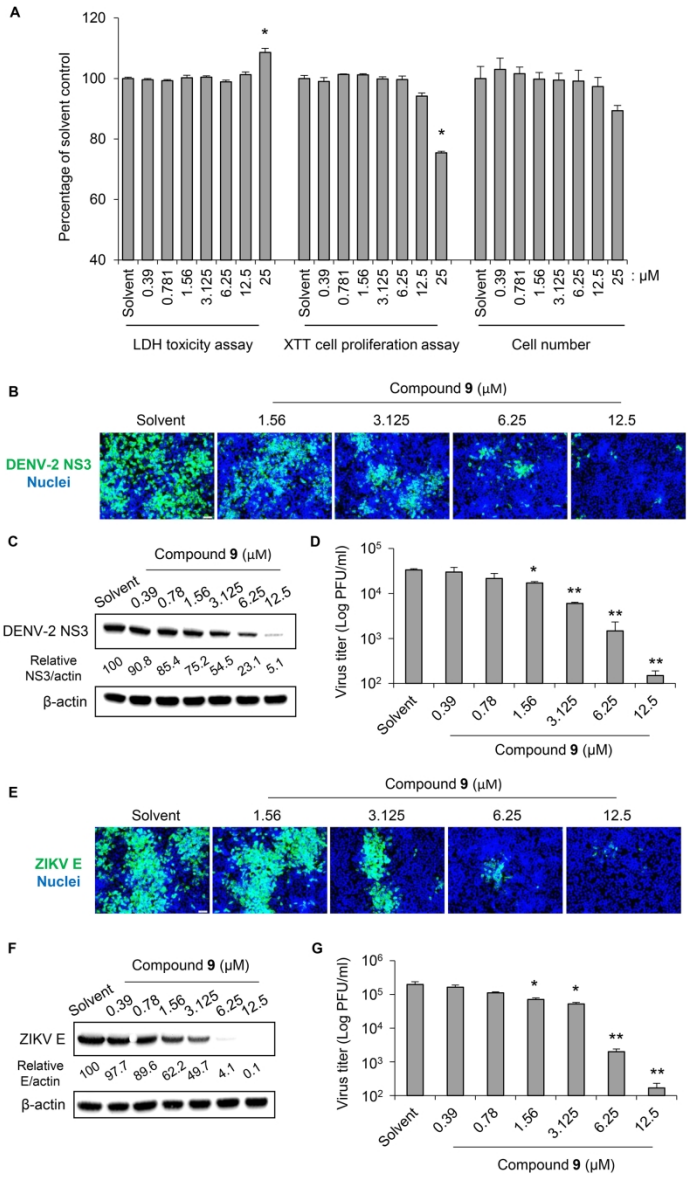

Figure 2. Determination of the cytotoxicity and antiviral activity of 9 against DENV-2 and ZIKV infection (multiplicity of infection [MOI], 0.1).

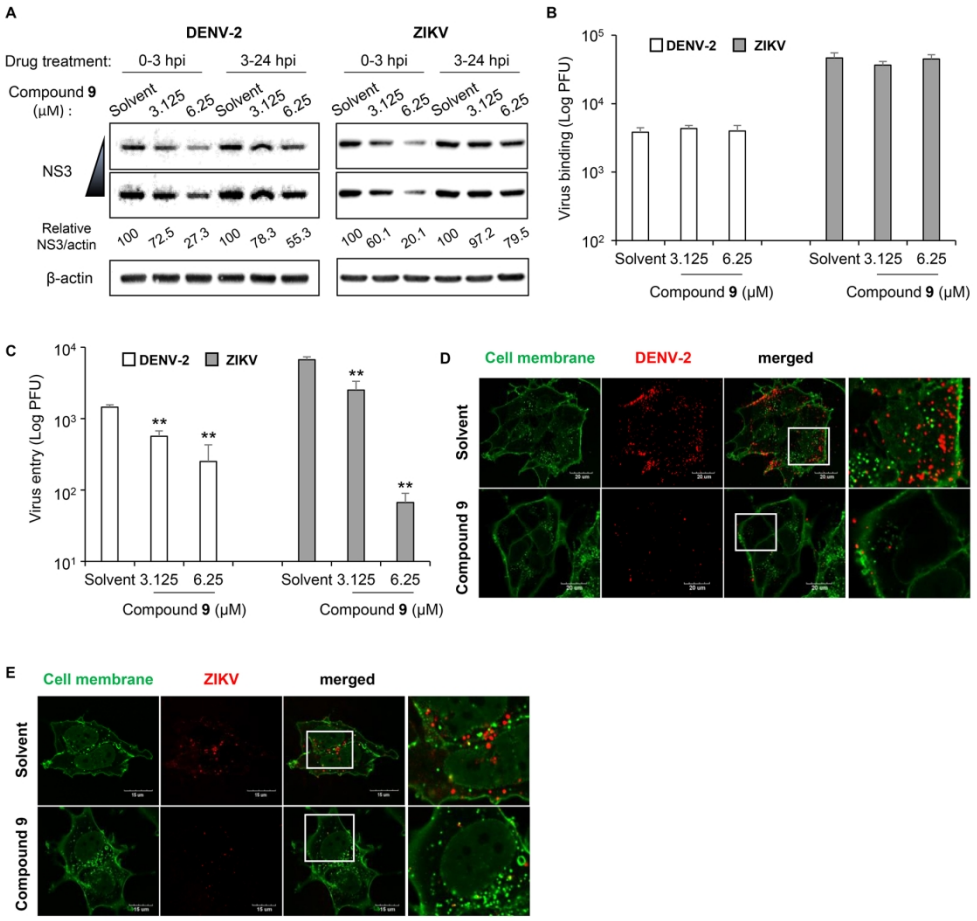

Figure 3. The effect of 9 on the DENV-2 and ZIKV cell binding and entry.

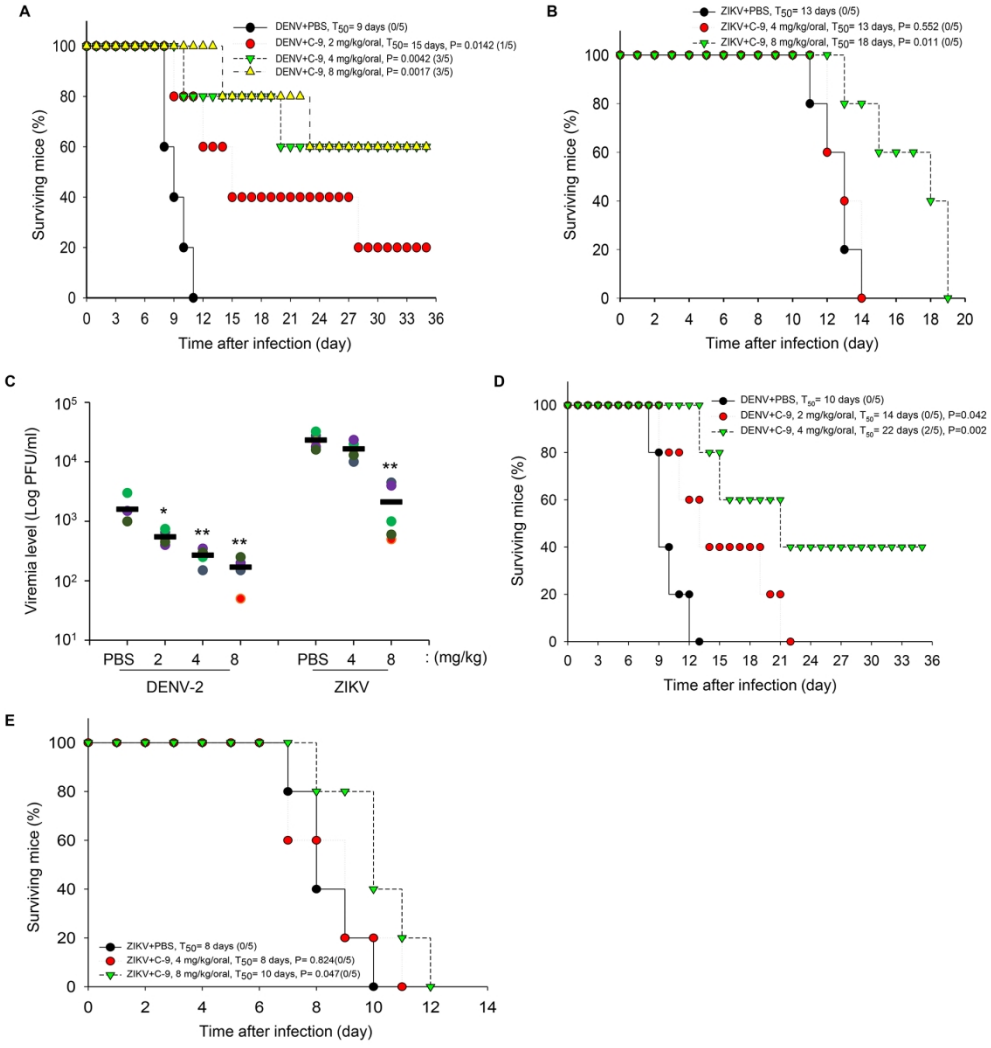

Figure 4. The impact of 9 on viral load and survival time for DENV-2 and ZIKV-infected Stat1-/- mice.

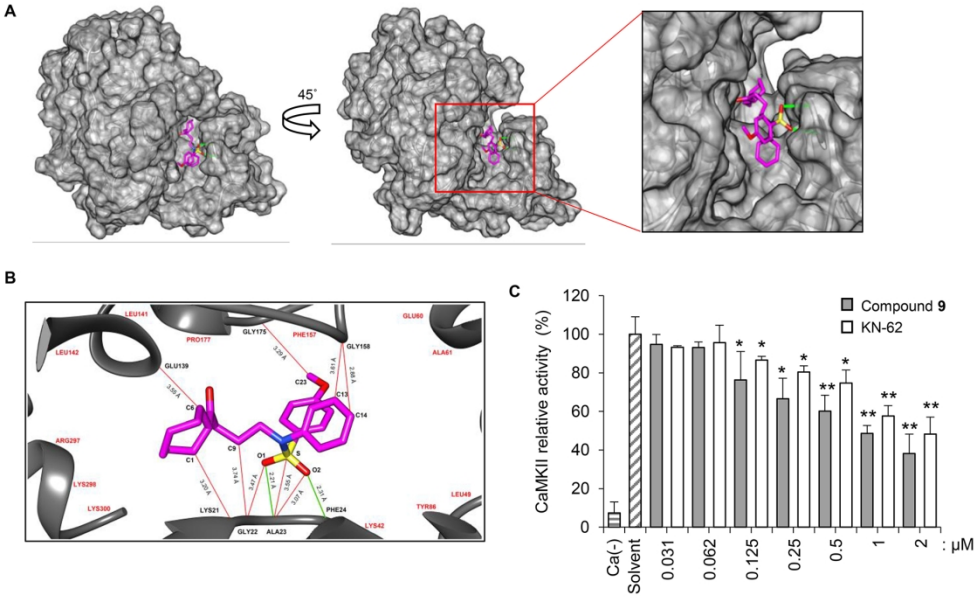

Figure 5. CaMKII-9 Molecular docking and inhibition.

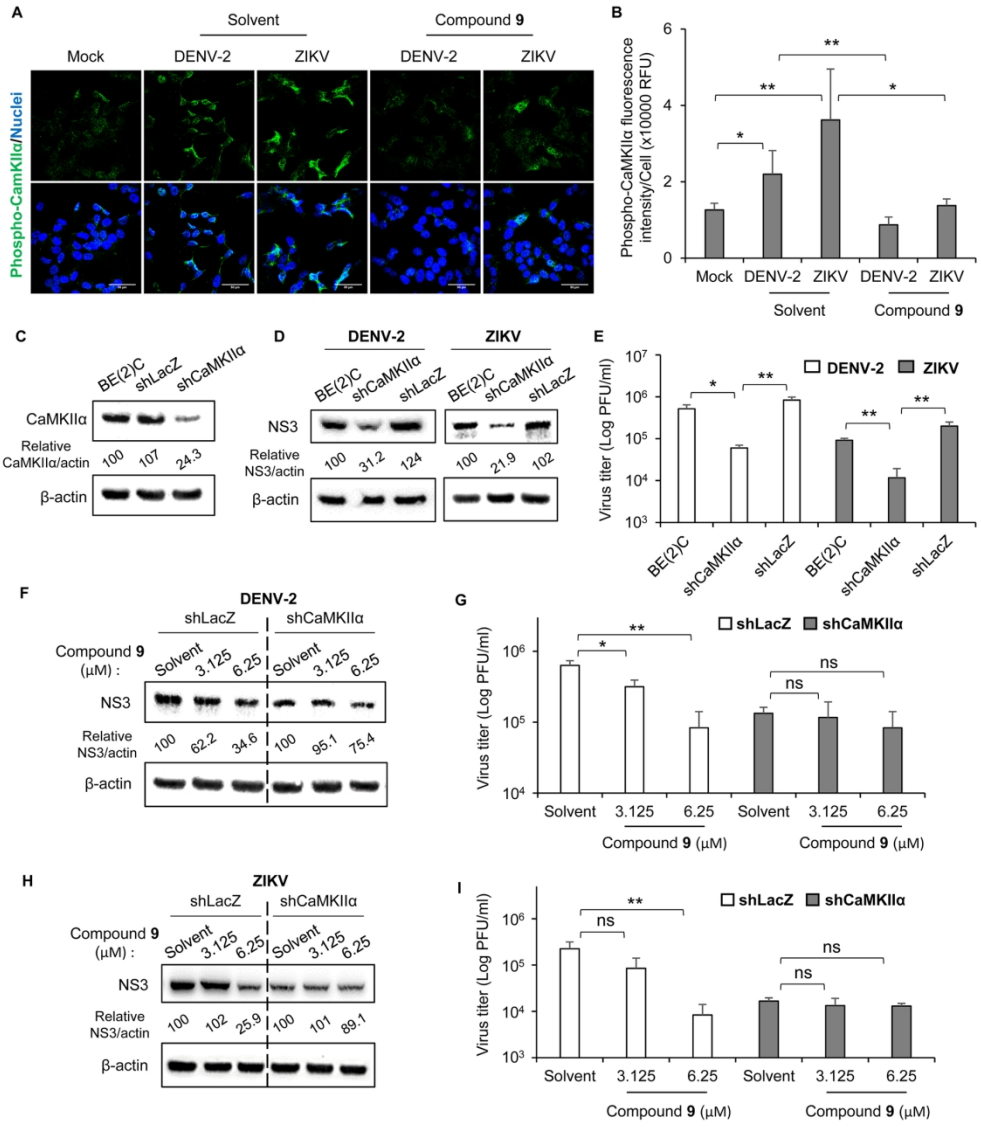

Figure 6. The antiviral activity of BSA9 is associated with CaMKIIα expression.

84x95mm (600 x 600 DPI)

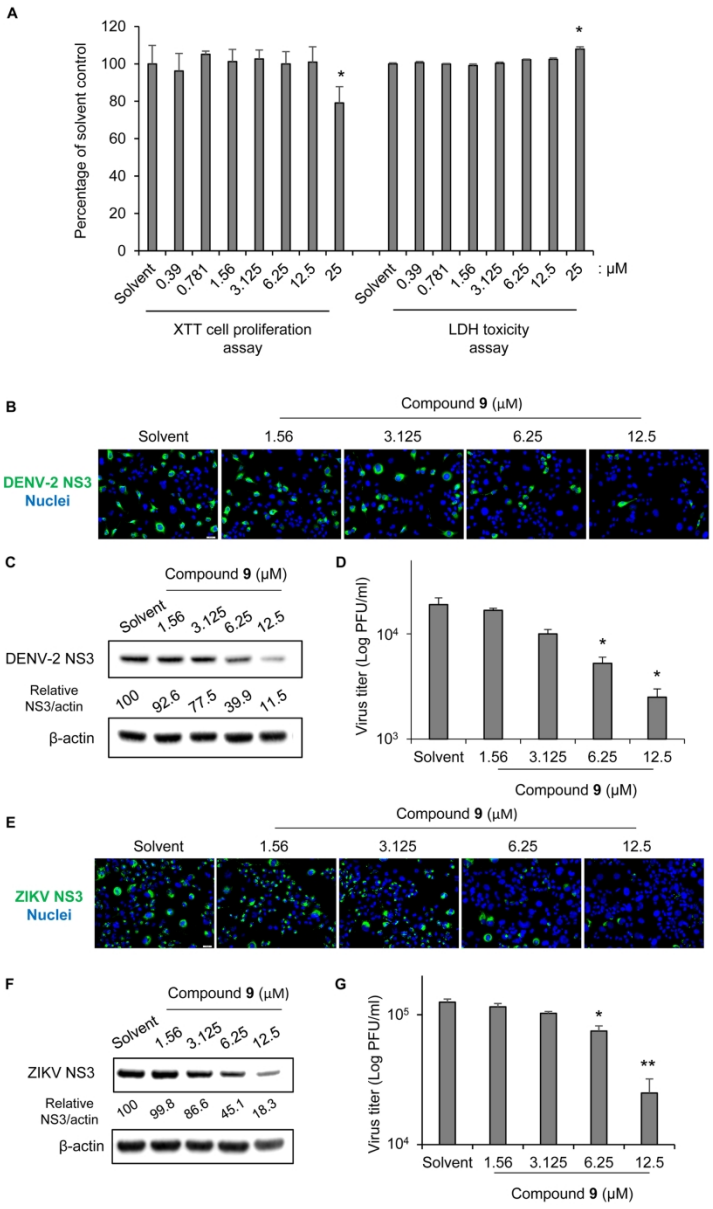

Figure S1. Determination of the cytotoxicity and antiviral activity of 9 against DENV-2 and ZIKV infection (multiplicity of infection [MOI], 1) in human microglial HMC3 cells.

84x137mm (600 x 600 DPI)

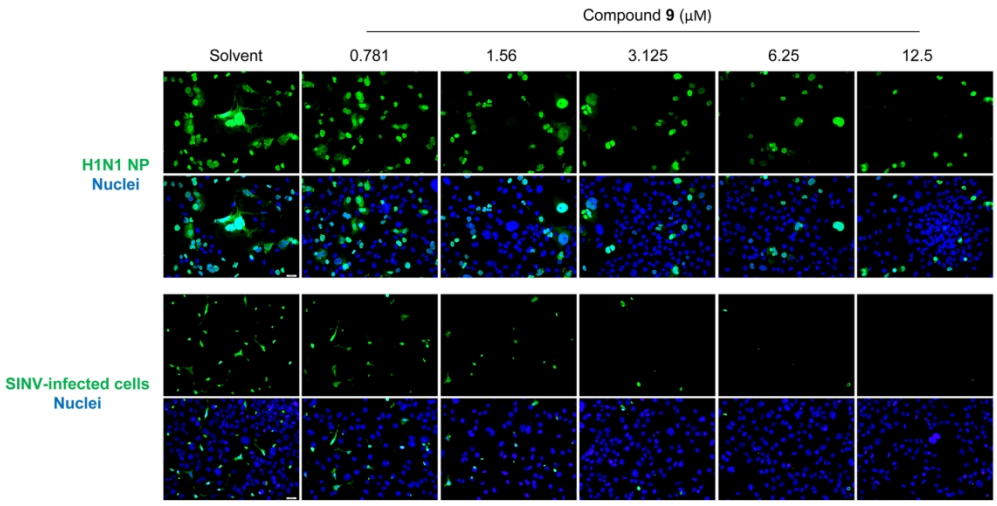

Figure S2. Antiviral activity of 9 against influenza H1N1 and Sindbis (SINV) virus infection.

84x42mm (600 x 600 DPI)

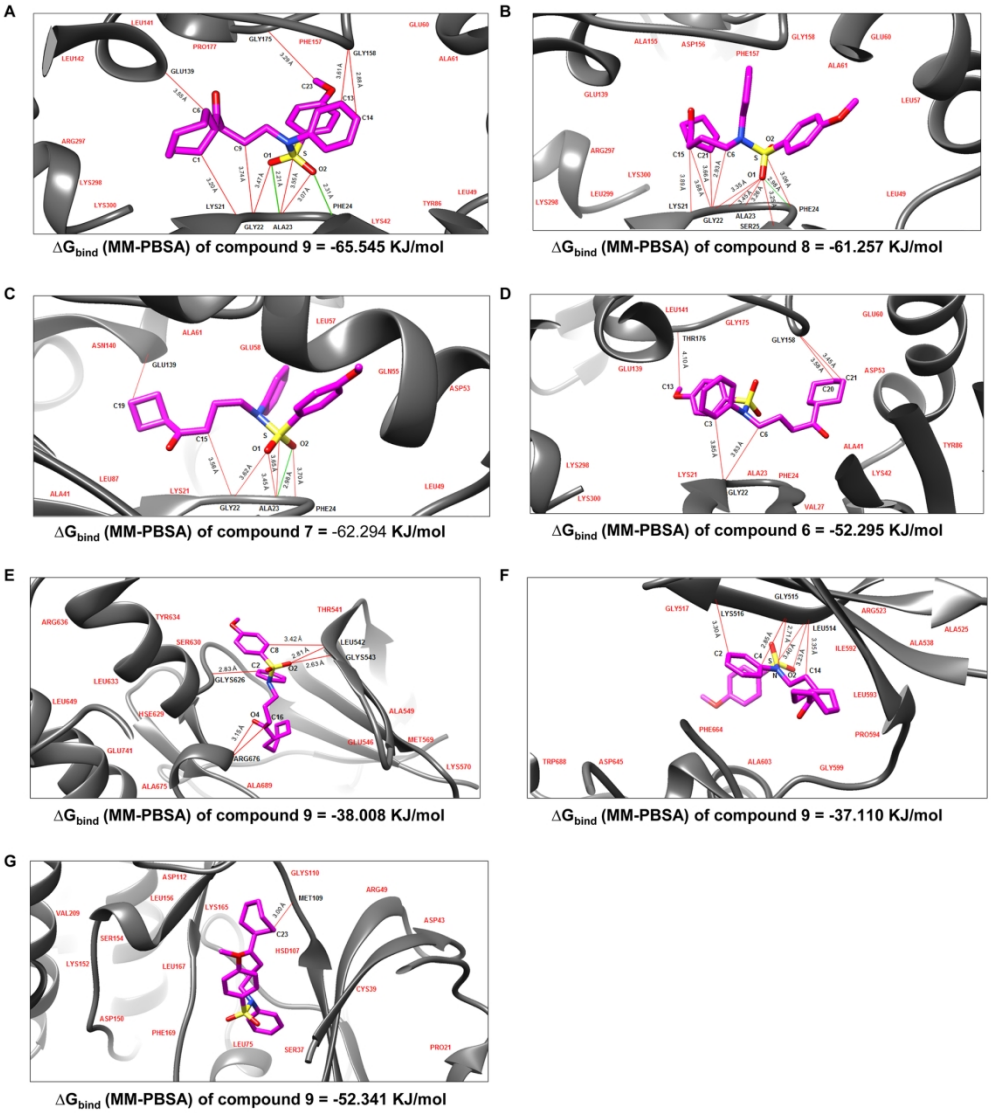

Figure S3. Molecular docking of BSA-kinases and the estimated binding free energy (MM/PBSA).

84x94mm (600 x 600 DPI)

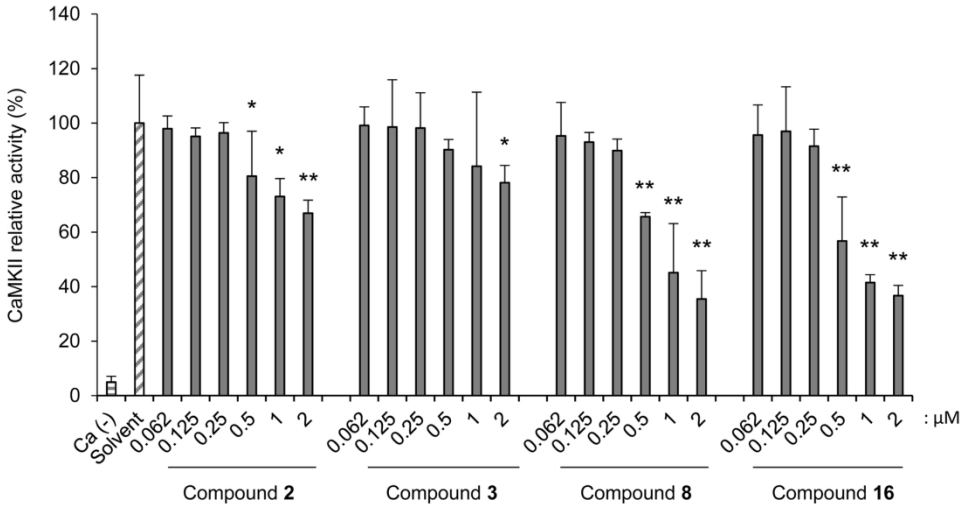

Figure S4. Biochemical assay of BSA 2, 3, 8, and 16 on human CaMKIIIα activity by use of CycLex CaM Kinase II assay.

84x45mm (600 x 600 DPI)